Manipulability Index Optimization for a Planar Robotic Arm

Max Engardt
Axel Heimbürger
Philip Sydhoff

Supervisors:
Johan Markdahl and Xiaoming Hu

Bachelor Thesis in Engineering Physics
Department of Mathematics, Division of Optimization and Systems Theory
KTH, Royal Institute of Technology
Stockholm, Sweden

May 21, 2012

Abstract

It is of interest to have high manipulability in robotic manipulators in order to achieve high performance. In this report, a model of a robotic arm manipulator is defined and analyzed with focus on optimizing the manipulability. The kinematics for the robotic manipulator is used to define quantitative measures of manipulability, *manipulability indices*. Analytical results for different manipulability indices are derived. It is shown that a common feature of the indices is that they are independent of the first angle of the robotic arm. Using numerical optimization, the *manipulability measure* is optimized under different constraints. The manipulability measure is also used when defining a path for the robotic arm manipulator with high manipulability. The path is described by polynomials in the *joint space*. Numerical optimization of the path is done for several examples. It is concluded that the indices give different measures of manipulability and are therefore suitable for different problems. It is also shown that the manipulability can be optimized when different constraints are imposed and that an optimal radius for the end-effector exists. Lastly, it is concluded that a short path with high manipulability is possible to obtain using the proposed method.

Nomenclature

$\boldsymbol{\theta}$	The joint variables
θ_i	The angle of the i:th joint
l_i	The length of the i:th link
$\mathcal{J}$	The joint space
$\mathcal{W}$	The workspace
$\mathcal{W}_D$	The dexterous workspace
$\mathcal{W}_R$	The reachable workspace
$\mathbf{p_e}$	The position of the end-effector
$\boldsymbol{\phi}_\mathbf{e}$	The orientation of the end-effector
$\mathbf{k}$	Forward kinematic function
$\mathbf{f}$	Position function
$\mathbf{v_e}$	Velocity of the end-effector
$\boldsymbol{\omega}_\mathbf{e}$	Angular velocity of the end-effector
$\mathbf{J}$	The Jacobian of the position function
$\mathbf{J}^\dagger$	The Moore-Penrose pseudo-inverse of $\mathbf{J}$
$\mathbf{J_P}$	Velocity decomposition of $\mathbf{J}$
$\mathbf{J_O}$	Angular velocity decomposition of $\mathbf{J}$
$\boldsymbol{\tau}$	The joint torques
$\boldsymbol{\gamma}_\mathbf{e}$	Sum of forces acting on the end-effector
$\mathbf{F_e}$	Force contribution on the end-effector
$\boldsymbol{\mu}_\mathbf{e}$	Moment contribution on the end-effector
μ	The manipulability measure

$\|\mathbf{J}\|_F$	The weighted Frobenius norm of $\mathbf{J}$
κ	The condition number
σ_{max}	The largest singular value of a matrix
σ_{min}	The smallest singular value of a matrix
λ_i	Eigenvalue i of a matrix
$\mathbf{u}_i$	Eigenvector i of a matrix
$\mathcal{F}$	The feasible set of an optimization problem
R	Radius from the origin of the robotic arm manipulator
$\mathbf{\Theta}$	The path-polynomial
a_{ij}	Coefficient for the path-polynomial
g	Objective function for the trajectory optimization problem

Contents

Chapter 1

Introduction

Robotic arm manipulators are frequently used in both industrial production but also in various other applications. Typical fields of usage for industrial robotic manipulators are material handling, machine tending, arc welding, cutting and product assembling with more examples to be found in [1]. Estimating and optimizing their performance is of importance both in theoretical studies and practical applications. The concept of manipulability is based on the ability to position and re-orientate the end-effector of the robotic arm in different directions. Optimizing the manipulability leads to increased performance for a robotic structure which can be used to design better robotic arms. The improvements in manipulability results in more versatile and supple robotic arms which is pursued by the industry, also mentioned in [1].

The robotic arm model considered in this report consists of rigid links attached by means of revolute joints i.e., joints restricted to turning in one dimension. The robotic arm model is planar meaning that the robotic arm only moves in a plane. Restricting the robotic arm to a plane has considerable advantages for the simplicity of the modeling and design of the arm. The planar model is frequently used and can be generalized to a three dimensional space by for example attaching the planar robotic manipulator to a mobile platform. Another options is to attach a revolute joint working in the complementary direction to the planar arm at the base of the manipulator. For an example of such a solution, see Figure 1.1.

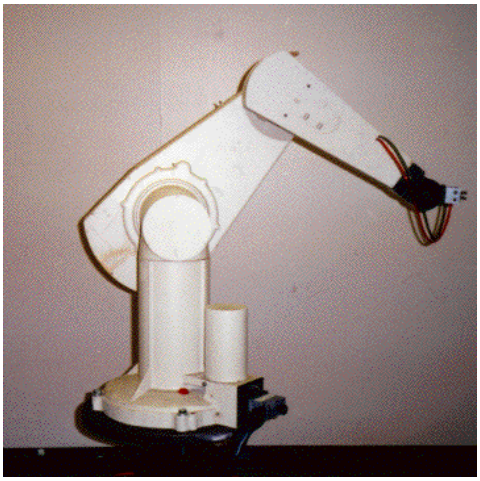

Figure 1.1: The PUMA 560, an example of a planar robotic arm manipulator.

In order to have a quantitative measure of the manipulability of a robotic arm certain robotic manipulability indices are introduced. Manipulability indices are not absolute and can be defined in various ways depending on the problem at hand. The considered indices in this report stems from the Jacobian matrix which describes the transformation between the angular velocities of the joints and the velocity of the end-effector. The Jacobian matrix constitutes a fundamental tool in the study of manipulability of robotic arms. Notably, it is used to analyze closeness to singular points. The Jacobian matrix is used both in the forward kinematic problem and in the inverse kinematic problem.

Optimizing the manipulability is done using numerical methods. These are performed using the optimization toolbox in MATLAB. The studied optimization problems are not convex but certainty of global optimality can still be assured for the solutions of the problems.

1.1 Outline of the Report

The report starts of with general theory regarding the robotic model and chosen manipulability indices which are presented and motivated. Relevant optimization theory is presented in Chapter 3, mainly for the unfamiliar reader. In Chapter 4 analytical results for the manipulability indices are derived. In Chapter 5 and Chapter 6 various optimization problems concerning manipulability indices are considered. Specifically, in Chapter 5, a three-link planar manipulator is studied and optimized for specific criterion. Lastly, in Chapter 6 a method for finding an optimal path is presented.

Chapter 2

Kinematics and Manipulability of the Robotic Arm

Manipulability indices associated with the end-effector of a robotic manipulator stems from the kinematics of the configuration. In order to introduce the manipulability indices, the kinematics of the robotic arm must thus first be established.

2.1 The Robotic Arm Model

This report will be restricted to the study of planar manipulators i.e., manipulators restricted to only move in a plane. The *manipulator* can be represented from a mechanical viewpoint as an assembly of rigid *links* connected by means of *joints*. The kinematic chain is the mathematical model of our mechanical system where one end of the chain is constrained to a base, while an *end-effector* is mounted to the other end. The joints can be designed in various ways but the focus will lie on so-called revolute joints which allow a relative rotation about a single axis per joint. The end-effector is used to manipulate objects in space. Therefore, it is the end-effector position and orientation, *pose*, that is often studied. Throughout this report, the robotic manipulator model will consist of a planar arm with n prismatic joints. The length of joint i is denoted as l_i and its angle by θ_i.

Definition 2.1. *The joint variables,* $\boldsymbol{\theta} = (\theta_1, ..., \theta_n)^T$*, are the angles of the prismatic joints.*

Figure 2.1 illustrates the above definition for a three-link planar arm. Introducing the joint variables, $\boldsymbol{\theta}$, allows for an easy description of the entire pose of the robot manipulator. Definition 2.1 enables one of the individual angles, $\theta_i, i = 1, \ldots, n$, to be changed independently.

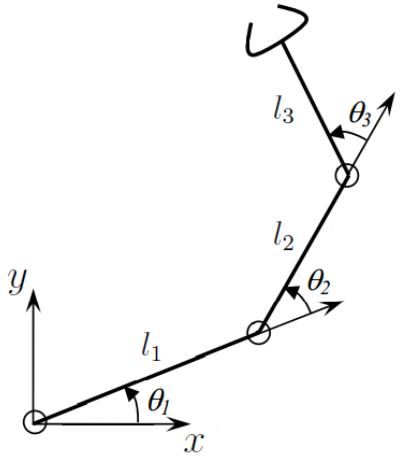

Figure 2.1: Schematic view of a three-link planar arm.

It will be useful to define the following spaces.

Definition 2.2. *The joint space, $\mathcal{J}$, is the space which consists of all possible configurations of the joint variables.*

Definition 2.3. *The workspace, $\mathcal{W}$, is the set of all possible end-effector positions.*

During this report the workspace will be a two-dimensional Cartesian space since only planar robotic arms are considered.

2.2 Forward Kinematics

Forward kinematics describes the pose of the end-effector as a function of the joint variables. The forward kinematic equation can be written as:

$$\mathbf{x_e} = \mathbf{k}(\boldsymbol{\theta}), \tag{2.1}$$

where $\mathbf{x_e}$ describes the pose. The non-linear vector function, $\mathbf{k}(\boldsymbol{\theta}) \in \mathbb{R}^m$, allows computation of the pose via the joint space variables. Here, m equals the least number of variables needed to describe the pose. However, if we want to execute time-dependent tasks it will be necessary to assign the end-effector position and orientation as a function of time.

A *minimal representation* is a parameterization using the minimum amount of parameters needed to express a specific system. With a minimal representation we can express the end effectors position and orientation using inherently independent variables. For detailed information, see for example [2]. By using a minimal representation we can describe the two elements in $\mathbf{x_e}$ separately. $\mathbf{x_e}$ can then be written as:

$$\mathbf{x_e} = \begin{pmatrix} \mathbf{p_e} \\ \phi_\mathbf{e} \end{pmatrix}, \tag{2.2}$$

where the vectors $\mathbf{p_e}$ and $\boldsymbol{\phi}_\mathbf{e}$ represents the end-effectors position and orientation respectively. The position, $\mathbf{p_e}$, is described via the position function. The position function, $\mathbf{f}(\boldsymbol{\theta})$, is the transformation of the end effectors position from joint variables to Cartesian coordinates for a planar manipulator.

Definition 2.4. *The position function,* $\mathbf{f}(\boldsymbol{\theta}) : \mathcal{J} \longrightarrow \mathcal{W}$*, is given by:*

$$\mathbf{p_e} = \mathbf{f}(\boldsymbol{\theta}) = \begin{pmatrix} \sum_{p=1}^{n} l_p \cos\left(\sum_{q=1}^{p} \theta_q\right) \\ \sum_{p=1}^{n} l_p \sin\left(\sum_{q=1}^{p} \theta_q\right) \end{pmatrix}. \tag{2.3}$$

The end-effector orientation, $\boldsymbol{\phi}_\mathbf{e}$, shall be fixed with respect to the joint configuration and is therefore given by:

$$\boldsymbol{\phi}_\mathbf{e} = \sum_{i=1}^{n} \theta_i. \tag{2.4}$$

Thus, the position in Cartesian coordinates and the orientation of the end-effector is calculated from the joint variables and the link lengths.

Two special workspaces shall be considered and are defined using forward kinematics:

Definition 2.5. *The reachable workspace for a planar manipulator, denoted* $\mathcal{W}_R$*, is the space which the end-effector can reach with at least one orientation and is defined as:*

$$\mathcal{W}_R = \{\mathbf{f}(\boldsymbol{\theta}) \in \mathbb{R}^2 \mid \boldsymbol{\theta} \in \mathcal{J}\}. \tag{2.5}$$

Definition 2.6. *The dexterous workspace for a planar manipulator, denoted* $\mathcal{W}_D$*, is defined as the space which the end-effector can reach with an arbitrary orientation or more formally:*

$$\mathcal{W}_D = \{\mathbf{p_e} \in \mathbb{R}^2 \mid \forall \boldsymbol{\varphi} \in \mathbf{SO}(2), \exists \boldsymbol{\theta} \in \mathcal{J} \text{ s.t. } \mathbf{k}(\boldsymbol{\theta}) = (\mathbf{p_e}, \boldsymbol{\varphi})\}. \tag{2.6}$$

The rotation group $\mathbf{SO}(2)$ can loosely be defined as all possible rotations in two dimensions. For a formal definition, see [3]. The dexterous workspace is convenient to use when considering task planning since it allows the orientation of the end-effector to be ignored when positioning objects.

In order to describe the differential kinematics, the Jacobian, $\mathbf{J}$ is introduced. The Jacobian describes a linear mapping from the joint velocity space to the end-effector velocity space. Using the Jacobian, the differential kinematic equation can be written as:

$$\begin{pmatrix} \mathbf{v_e} \\ \boldsymbol{\omega}_\mathbf{e} \end{pmatrix} = \mathbf{J}(\boldsymbol{\theta})\dot{\boldsymbol{\theta}}, \tag{2.7}$$

where:

$$\begin{cases} \mathbf{v_e} = \dot{\mathbf{p}}_\mathbf{e}, \\ \boldsymbol{\omega}_\mathbf{e} = \dot{\boldsymbol{\phi}}_\mathbf{e}. \end{cases} \tag{2.8}$$

The Jacobian, $\mathbf{J}(\boldsymbol{\theta})$, can be decomposed as:

$$\mathbf{J} = \begin{pmatrix} \mathbf{J_P} \\ \mathbf{J_O} \end{pmatrix}. \tag{2.9}$$

Decomposing $\mathbf{J}$ into $\mathbf{J_P}$ and $\mathbf{J_O}$ allows us to rewrite expression (2.7) as:

$$\begin{cases} \mathbf{v_e} = \mathbf{J_P}\dot{\boldsymbol{\theta}}, \\ \boldsymbol{\omega_e} = \mathbf{J_O}\dot{\boldsymbol{\theta}}. \end{cases} \tag{2.10}$$

Henceforth, $\mathbf{J_P}$ shall be denoted simply as $\mathbf{J}$ since the angle $\boldsymbol{\phi_e}$ shall be fixed with respect to the robotic arm. $\mathbf{J}$ is the Jacobian of the position function and is given by:

$$\mathbf{J} = \frac{\partial \mathbf{f}}{\partial \boldsymbol{\theta}} = \begin{pmatrix} \sum_{i=1}^{n} -l_i \sin\left(\sum_{k=1}^{i} \theta_k\right) & \cdots & \sum_{i=n}^{n} -l_i \sin\left(\sum_{k=1}^{i} \theta_k\right) \\ \sum_{i=1}^{n} l_i \cos\left(\sum_{k=1}^{i} \theta_k\right) & \cdots & \sum_{i=n}^{n} l_i \cos\left(\sum_{k=1}^{i} \theta_k\right) \end{pmatrix}. \tag{2.11}$$

2.3 Inverse Kinematics

The forward kinematics function, $\mathbf{k}(\boldsymbol{\theta})$, relates the joint variables to a specific pose. The *inverse kinematic problem* consists of finding the inverse relationship i.e., the determination of the joint variables corresponding to a given end-effector position and orientation. In practice, it is often this relationship which is interesting since the task to be performed is typically specified in $\mathcal{W}$. The solution to this problem is fundamental in order to transform the motion specifications, assigned in $\mathcal{W}$, to the corresponding joint space motion configuration.

The inverse kinematic problem is more complex compared to the forward kinematic problem. Once the joint variables are known in the forward kinematic equation the end-effector position and orientation are computed in a unique manner. However, the inverse kinematic problem generally does not share the same uniqueness property. There may exist multiple, infinitely many or zero solutions. The existence of solutions is guaranteed only if the given end-effector position belong to the manipulators dexterous workspace, as mentioned in [2]. There exist infinitely many solutions in the case of kinematic redundancy i.e., the robotic arm has more degrees of freedom than needed to perform a specific task. In the case of multiple or infinitely many solutions we may reduce the number of feasible solutions by adding various constraints and criterion such as mechanical joint limits.

It will be necessary to find the inverse of the Jacobian matrix when solving the inverse kinematics problem. In the case where the Jacobian matrix is square and invertible the inverse can be calculated in the usual sense. However, if the Jacobian does not fulfill this, which is common, we still need to find some alternative form of the inverse. This report will consider Jacobian matrices of full row rank with the number of links more than or equal to two. For such Jacobian matrices the following definition holds:

Definition 2.7. *The Moore-Penrose pseudo-inverse* $\mathbf{J}^\dagger$ *of* $\mathbf{J}$ *solves the differential kinematic equation for* $\dot{\boldsymbol{\theta}}$ *while minimizing* $\|\dot{\boldsymbol{\theta}}\|$.

Thus, the Moore-Penrose pseudo inverse solves the following:

$$\mathbf{v_e} = \mathbf{J}(\boldsymbol{\theta})\dot{\boldsymbol{\theta}} \Rightarrow \dot{\boldsymbol{\theta}} = \mathbf{J}^\dagger \mathbf{v_e}. \tag{2.12}$$

The Moore-Penrose pseudo-inverse is a generalization of the usual matrix inverse and is unique for every matrix. For invertible square matrices it holds that $\mathbf{J}^\dagger = \mathbf{J^{-1}}$. In the case of three or more links, the term $\mathbf{J}^\dagger \mathbf{v_e} \in \mathcal{N}^\perp(\mathbf{J}) \equiv \mathcal{R}(\mathbf{J}^T)$ minimizes the norm of $\|\dot{\boldsymbol{\theta}}\|$. Jacobian matrices

with more columns than rows which have full row-rank shall be studied. A useful identity for the Moore-Penrose pseudo-inverse for such matrices can, according to [4], be written as:

$$\mathbf{J}^{\dagger} = \mathbf{J}^{T}(\mathbf{J}\mathbf{J}^{T})^{-1}. \tag{2.13}$$

This identity shall be useful when deriving the expressions for the manipulability ellipsoids.

2.4 Static Equilibrium of Forces

Statics determines the connection between the generalized forces applied to the end-effector and the generalized forces applied to the joints when the manipulator is at an equilibrium configuration. The generalized forces applied to the joints are torques in the case of revolute joints, denoted by the vector $\boldsymbol{\tau} \in \mathbb{R}^n$, where n is the number of joints. The end-effector forces are denoted by the vector $\boldsymbol{\gamma}_{\mathbf{e}} \in \mathbb{R}^r$, where r equals the number of variables needed to describe the pose of the end-effector. Mechanical manipulator systems which are time-invariant and path-independent are considered in this report. The configuration thus only depends on the joint variables, $\boldsymbol{\theta}$, and not explicitly on time.

In order to establish a relationship between the end-effector forces and the joint torques we shall consider the elementary works by the two force systems. The elementary work associated with the joint torques, $dW_{\boldsymbol{\tau}}$, can according to [4] be written as:

$$dW_{\boldsymbol{\tau}} = \boldsymbol{\tau}^{T} d\boldsymbol{\theta}. \tag{2.14}$$

The end-effector forces, $\boldsymbol{\gamma}_{\mathbf{e}}$, can be divided into two contributions; the moment contribution, $\boldsymbol{\mu}_{\mathbf{e}}$, and the force contribution, $\mathbf{F}_{\mathbf{e}}$, and thus:

$$\boldsymbol{\gamma}_{\mathbf{e}} = \begin{pmatrix} \mathbf{F}_{\mathbf{e}} \\ \boldsymbol{\mu}_{\mathbf{e}} \end{pmatrix}. \tag{2.15}$$

The elementary work associated with the moment and force contribution is:

$$dW_{\boldsymbol{\gamma}} = \mathbf{F}_{\mathbf{e}}^{T} d\mathbf{p}_{\mathbf{e}} + \boldsymbol{\mu}_{\mathbf{e}}^{T} \boldsymbol{\omega}_{\mathbf{e}} dt. \tag{2.16}$$

Using equation (2.8) and (2.10), equation (2.16) can be written as:

$$dW_{\boldsymbol{\gamma}} = \mathbf{F}_{\mathbf{e}}^{T} \mathbf{J}_{\mathbf{P}} d\boldsymbol{\theta} + \boldsymbol{\mu}_{\mathbf{e}}^{T} \mathbf{J}_{\mathbf{O}} d\boldsymbol{\theta} = \boldsymbol{\gamma}_{\mathbf{e}}^{T} \mathbf{J} d\boldsymbol{\theta}. \tag{2.17}$$

At static equilibrium, the end-effector forces balances out, $dW_{\boldsymbol{\tau}} = dW_{\boldsymbol{\gamma}}$. Inserting equation (2.14) and (2.17) in the previous relation yields:

$$\boldsymbol{\tau}^{T} d\boldsymbol{\theta} = \boldsymbol{\gamma}_{\mathbf{e}}^{T} \mathbf{J} d\boldsymbol{\theta} \Rightarrow \boldsymbol{\tau} = \mathbf{J}^{T} \boldsymbol{\gamma}_{\mathbf{e}}. \tag{2.18}$$

This is a useful result which relates the end-effector forces and the joint torques by means of the transpose of the Jacobian. This relation will later be used when deriving the expression for the force ellipsoid.

2.5 Kinematic Singularities

There exist certain points in the joint space, $\mathcal{J}$, where the kinematic Jacobian, $\mathbf{J}$, locally has reduced rank. These points are called *singular points* and movement is limited to fewer dimensions. For a planar robotic arm the movement is thus reduced to only one dimension. In [2],

it is discussed that in the vicinity of singular points small velocities in the workspace leads to very large velocities in the joint space which is not preferable. Avoiding singular points, where the manipulability is greatly reduced, is thus very important. *Boundary singularities* occurs when the robotic arm is completely outstretched and the links are collinear. The boundary singularities can be avoided by reducing the allowed workspace to be confined within reachable workspace. *Internal singularities* occur within the reachable workspace and are harder to avoid. They generally occur due to unfortunate joint configurations where the links are coaxial.

2.6 Manipulability Indices

The purpose of manipulability indices is to give a quantitative measure of the ability to move and apply forces in arbitrary directions. The defined manipulability indices should also give information about the proximity of singular configurations. There exist multiple ways of defining manipulability giving rise to multiple manipulability indices. For more examples of manipulability indices than discussed in this report, see [5].

Definition 2.8. *The manipulability measure based on the Jacobian matrix,* $\mathbf{J}$*, is defined as:*

$$\mu(\boldsymbol{\theta}) = \sqrt{\det(\mathbf{J}\mathbf{J}^T)}. \tag{2.19}$$

The manipulability measure $\mu \in \mathbb{R}^+$ since the matrix $\mathbf{J}\mathbf{J}^T$ is positive semi-definite. For reference, see [6]. The manipulability measure was introduced by T. Yoshikawa, [7], and is widely used in robotic studies. Larger values of μ represents greater freedom for the specific configuration. The manipulability measure provides a measure of the product of the eigenvalues of $\mathbf{J}\mathbf{J}^T$.

Another measure of manipulability is the *weighted Frobenius norm* of a the Jacobian matrix $\mathbf{J}$:

Definition 2.9. *The weighted Frobenius norm of* $\mathbf{J}$ *is equal to:*

$$\|\mathbf{J}\|_F(\boldsymbol{\theta}) = \sqrt{\frac{1}{n}\operatorname{tr}(\mathbf{J}\mathbf{J}^T)}, \tag{2.20}$$

where n *equals the dimension of the workspace.*

The weighted Frobenius norm provides a measure of the sum of the eigenvalues of the matrix $\mathbf{J}\mathbf{J}^T$. For more details, see [4].

2.7 Manipulability Ellipsoids

A commonly used measure of manipulability are the manipulability ellipsoids. Both the so-called *velocity manipulability ellipsoid* as well as the *force manipulability ellipsoid* will be studied.

2.7.1 The Velocity Manipulability Ellipsoid

The *velocity manipulability ellipsoid* is a representation of the ability for the manipulator to change its end-effector position. The expression for the velocity manipulability ellipsoid is derived below, for more background, see [8].

Consider the set of joint velocities with constant unit norm i.e., a unit sphere in the joint velocity space:

$$\dot{\boldsymbol{\theta}}^T \dot{\boldsymbol{\theta}} = 1. \tag{2.21}$$

Inserting the expression for the differential kinematics solved for the joint velocities, (2.12), and later using (2.13) in (2.21) gives:

$$\begin{aligned}(\mathbf{J}^\dagger \mathbf{v_e})^T (\mathbf{J}^\dagger \mathbf{v_e}) &= \mathbf{v_e}^T (\mathbf{J}^T (\mathbf{J}\mathbf{J}^T)^{-1})^T \cdot \mathbf{J}^T (\mathbf{J}\mathbf{J}^T)^{-1} \mathbf{v_e} \\ &= \mathbf{v_e}^T (\mathbf{J}\mathbf{J}^T)^{-T} \mathbf{J}\mathbf{J}^T (\mathbf{J}\mathbf{J}^T)^{-1} \mathbf{v_e} \\ &= \mathbf{v_e}^T (\mathbf{J}\mathbf{J}^T)^{-1} \mathbf{v_e} \\ &= 1. \end{aligned} \tag{2.22}$$

The expression above defines the points on the surface of an ellipsoid in the end-effector velocity space. The shape and size of the ellipsoid is given by (2.22). The directions of the principal axes of the ellipsoid is given by the direction of the eigenvectors of $\mathbf{J}\mathbf{J}^T$ and the lengths of the axes by the square root of the eigenvalues. For more details, see Appendix A. In the case of a planar manipulator, $\mathbf{J}\mathbf{J}^T$ has two orthogonal eigenvectors with corresponding eigenvalues.

The manipulability ellipsoid provides an intuitive and easily illustrated perception of the ability for the configuration to move in a certain direction, see Figure 2.2 for an example. A large singular value indicates high manipulability in the corresponding direction. The velocity manipulability ellipsoid also indicates how near we are a singular configuration since one of the axes of the ellipsoid will converge towards zero. This characteristic of the manipulability ellipsoid leads to the concept of the *condition number* of a configuration.

Definition 2.10. *The condition number, κ, is defined as the ratio of the smallest and the largest singular value of $\mathbf{J}\mathbf{J}^T$. Let σ_{max} denote the largest singular value and σ_{min} the smallest. Then:*

$$\kappa = \frac{\sigma_{min}}{\sigma_{max}} = \{\mathbf{J}\mathbf{J}^T \geq 0\} = \sqrt{\frac{\lambda_{min}}{\lambda_{max}}}. \tag{2.23}$$

If the value of the condition number, κ, is close to one, we have an isotropic ellipsoid which indicates that the ellipsoid is shaped similarly to a sphere. On the other hand, if the value of κ is small, it indicates closeness to a singular point. Having an isotropic ellipsoid is preferable if high manipulability in many directions is desired. Because of these properties, the condition number, κ, shall be studied as a manipulability index.

There exists clear connections between the proposed manipulability indices and the manipulability ellipsoids besides the condition number. The manipulability measure, μ, describes the product of the principal axes and is thus proportional to the volume of the ellipsoid, see Appendix B for details. The weighted Frobenius norm $\|\mathbf{J}\|_F$ represents the sum of the lengths of the axes.

2.7.2 The Force Manipulability Ellipsoid

An additional description of the manipulability of a structure can be made using forces instead of velocities. This is possible due to the relation between differential kinematics and statics, for further background, see [9]. The derivation and results of the force manipulability ellipsoid are similar to those of the velocity ellipsoid. Consider the unit sphere in the space of joint torques:

$$\boldsymbol{\tau}^T \boldsymbol{\tau} = 1. \tag{2.24}$$

Inserting the static relationship between the joint torques and the end-effector forces, (2.18), yields:

$$\boldsymbol{\gamma}_\mathbf{e}^T (\mathbf{J}\mathbf{J}^T) \boldsymbol{\gamma}_\mathbf{e}^T = 1. \tag{2.25}$$

The expression above maps the unit sphere of joint torques into an ellipsoid in the space of end-effector forces. The force manipulability ellipsoid describes the end-effector forces that can be generated with the given set of joint torques for a certain manipulator posture.

The similarity between the velocity manipulability ellipsoid, given by (2.22), and the force ellipsoid, (2.25), is clear. The direction and shape of the force manipulability ellipsoid is given by the eigenvalues and eigenvectors of $(\mathbf{J}\mathbf{J}^T)^{-1}$. The eigenvectors, are thus equal to those of the velocity ellipsoid but the eigenvalues are reciprocal to those of the velocity ellipsoid. The principal axes of the force manipulability ellipsoid thus coincide with the axes of the velocity manipulability ellipsoid but the lengths of the axes are of inverse proportion. This leads to the conclusion that for non-isotropic configurations the direction along which good velocity manipulability is obtained is also a direction with low force manipulability, and vice versa. For an illustration of the two ellipsoids, see Figure 2.2.

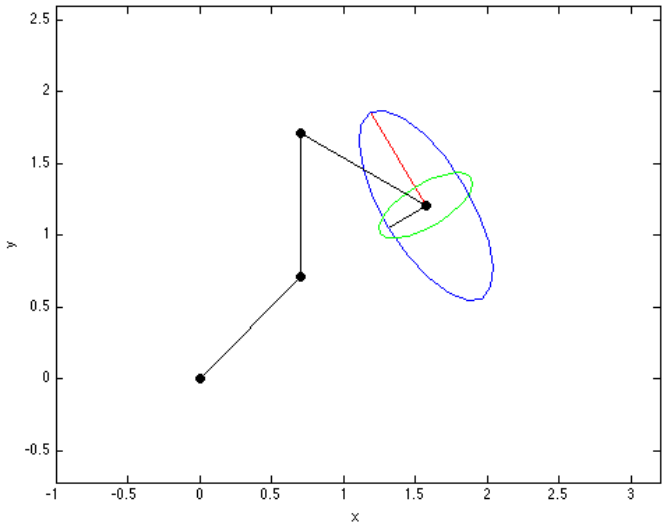

Figure 2.2: An example of the velocity manipulability ellipsoid, displayed in blue, and force ellipsoid, displayed in green for a three link planar arm. The principal axes are pictured for the velocity manipulability ellipsoid.

Chapter 3

Optimization Theory

In later chapters of this project different kinds of optimization problems will be studied. In Chapter 5, optimization problems related to maximizing the manipulability will be considered. In Chapter 6, the aim will be to optimize the trajectory of the end-effector when taking into consideration the manipulability and length of the trajectory. To understand the problem formulations in these chapters some basic definitions will be introduced. For more detailed information regarding the optimization theory presented in this chapter, see [10].

3.1 Basic Optimization Definitions

The optimization problems encountered in this report can all be written on the form (3.1):

$$\begin{bmatrix} \min & f(\mathbf{x}) \\ \text{s.t.} & \mathbf{x} \in \mathcal{F} \end{bmatrix}. \tag{3.1}$$

Below follows the definitions for the various parts of this problem together with how they relate to the problems encountered in this report.

Definition 3.1. *The objective function, $f : \mathbb{R}^n \longrightarrow \mathbb{R}$, is the object of the optimization i.e., the function to minimize.*

In this report, the objective function will either be a manipulability index or a function describing the trajectory.

Definition 3.2. *The variables, $\mathbf{x} \in \mathbb{R}^n$, is what the objective function will be optimized with regards to.*

The variables will be either the joint variables or parameters governing the path in joint space.

Definition 3.3. *The feasible set, $\mathcal{F}$, is the set containing all the allowed values of the variables.*

Since $\mathbf{x} \in \mathbb{R}^n$ it follows that $\mathcal{F} \subseteq \mathbb{R}^n$.

Definition 3.4. *A point $\mathbf{x}$ is said to be a feasible solution if $\mathbf{x} \in \mathcal{F}$.*

Note that only looking at minimization problems is not a loss of generality. Maximization problems are easily transformed into minimization problems by changing objective function, f, to $-f$. This will later be used since problems of maximizing the manipulability shall be considered.

The solution to an optimization problem is called the *optimal solution* and the value of the objective function at the optimal solution is called the *optimal value*. For a vector $\hat{\mathbf{x}}$ to be an optimal solution it must hold that:

$$\begin{aligned} \hat{\mathbf{x}} &\in \mathcal{F}, \\ f(\hat{\mathbf{x}}) &\leq f(\mathbf{x}), \forall \mathbf{x} \in \mathcal{F}. \end{aligned} \tag{3.2}$$

One important theorem that guaranties a global optimal solution is stated below. This will be applicable later to ensure that a global optimal solution to the problems stated exists.

Theorem 3.1. *Suppose f is a continuous real function on a nonempty compact set $X \subseteq \mathbb{R}^n$, then there exists $x_1, x_2 \in X$ such that:*

$$\begin{aligned} f(x_1) &= \max_{x \in X} f(x) = \sup_{x \in X} f(x), \\ f(x_2) &= \min_{x \in X} f(x) = \inf_{x \in X} f(x), \end{aligned}$$

where sup denotes the least upper bound and inf denotes the greatest lower bound.

For proof of this theorem, see [11].

3.2 The Feasible Set

The general feasible set is constructed by constraints that depend on the problem. The feasible set can be defined as:

$$\mathcal{F} = \{\mathbf{x} \in \mathbb{R}^n \mid g_i(\mathbf{x}) \leq 0, i = 1, \ldots, m\}, \tag{3.3}$$

where $g_1(\mathbf{x}), ..., g_m(\mathbf{x})$ are functions $\mathbb{R}^n \longrightarrow \mathbb{R}$. The constraints are continuously differentiable. Constraints on this form will be encountered later for example when the arm is constrained to a specific radius.

One important special case for the feasible set is when the constraints are linear. Then, the feasible set can be simplified to:

$$\mathcal{F} = \{\mathbf{x} \in \mathbb{R}^n \mid \mathbf{A}\mathbf{x} \leq \mathbf{b}\}. \tag{3.4}$$

This will be the case when considering constraints on the joint variables and the parameters involved in the trajectory optimization. In (3.4), the constraints have been simplified using a matrix $\mathbf{A} \in \mathbb{R}^{m \times n}$ and a vector $\mathbf{b} \in \mathbb{R}^m$ where m is the number of constraints.

3.3 Convexity

A pleasant property of an optimization problem is when it is convex. This guaranties that a local minimum also is a global minimum. Below follows the formal definitions. In Chapter 4, it will be shown that the manipulability measure, μ, is not convex.

Definition 3.5. *A set, S, is convex if, for any x and y in S the following holds: $\alpha x + (1-\alpha)y \in S$, for all $\alpha \in [0, 1]$.*

Definition 3.6. *A function f is convex on a convex set S if for all x and y in S and for all $\alpha \in [0, 1]$ the following holds: $f(\alpha x + (1-\alpha)y) \leq \alpha f(x) + (1-\alpha)f(y)$.*

Definition 3.7. *An optimization problem is said to be convex if the objective function is a convex function and the feasible set is a convex set.*

Chapter 4

Analytical Results for Manipulability Indices

In the following chapter, three different manipulability indices will be considered and it will be shown that their value always is independent of the first angle, θ_1. The robotic arm in this chapter is consistent with the model described in Chapter 2. Proving the independence of the first angle is essential in further analysis of the subject since θ_1 may be disregarded from the objective function of the optimization. Some other properties of the indices are also discussed.

4.1 The Weighted Frobenius Norm

Recall the definition of the weighted Frobenius norm defined in Chapter 2:

$$\|\mathbf{J}\|_F = \sqrt{\frac{1}{n}\operatorname{tr}(\mathbf{J}\mathbf{J}^T)}. \tag{4.1}$$

4.1.1 First Angle Independence

Theorem 4.1. *The weighted Frobenius norm of a planar robotic arm is independent of the first angle, θ_1 and is given by:*

$$\|\mathbf{J}\|_F = \sqrt{\frac{1}{2}\sum_{i=1}^{n} i l_i^2 + \sum_{i=1}^{n-1}\sum_{p=i}^{n}\sum_{m=i+1}^{n} l_p l_m \cos\left(\sum_{q=p+1}^{m}\theta_q\right)}. \tag{4.2}$$

Proof. For simplicity, the following notations for the workspace coordinates are introduced. The notation will be used throughout this chapter:

$$\begin{cases} x = \sum_{p=1}^{n} l_p \cos\left(\sum_{q=1}^{p}\theta_q\right), \\ y = \sum_{p=1}^{n} l_p \sin\left(\sum_{q=1}^{p}\theta_q\right). \end{cases} \tag{4.3}$$

Considering equation (4.3), note that the following hold for $i = 1, \ldots, n$:

$$\begin{cases} \frac{\partial x}{\partial \theta_i} = -\sum_{p=i}^{n} l_p \sin\left(\sum_{q=1}^{p} \theta_q\right), \\ \frac{\partial y}{\partial \theta_i} = \sum_{p=i}^{n} l_p \cos\left(\sum_{q=1}^{p} \theta_q\right). \end{cases} \tag{4.4}$$

Using the notations defined in (4.3), $\mathbf{J}$ may be written in a compact form:

$$\mathbf{J} = \begin{pmatrix} \frac{\partial x}{\partial \theta_1} & \cdots & \frac{\partial x}{\partial \theta_n} \\ \frac{\partial y}{\partial \theta_1} & \cdots & \frac{\partial y}{\partial \theta_n} \end{pmatrix}. \tag{4.5}$$

By matrix multiplication and introducing one more summation, an expression for $\mathbf{J}\mathbf{J}^T$ is obtained:

$$\mathbf{J}\mathbf{J}^T = \begin{pmatrix} \sum_{i=1}^{n} \left(\frac{\partial x}{\partial \theta_i}\right)^2 & \sum_{i=1}^{n} \frac{\partial x}{\partial \theta_i}\frac{\partial y}{\partial \theta_i} \\ \sum_{i=1}^{n} \frac{\partial x}{\partial \theta_i}\frac{\partial y}{\partial \theta_i} & \sum_{i=1}^{n} \left(\frac{\partial y}{\partial \theta_i}\right)^2 \end{pmatrix}. \tag{4.6}$$

To prove that the weighted Frobenius norm is independent of θ_1, it is sufficient to prove that the trace of $\mathbf{J}\mathbf{J}^T$ is independent of θ_1. The trace of $\mathbf{J}\mathbf{J}^T$ is expressed as following:

$$\begin{aligned} \operatorname{tr}(\mathbf{J}\mathbf{J}^T) &= \mathbf{J}\mathbf{J}_{1,1}^T + \mathbf{J}\mathbf{J}_{2,2}^T \\ &= \sum_{i=1}^{n} \left(\frac{\partial x}{\partial \theta_i}\right)^2 + \sum_{i=1}^{n} \left(\frac{\partial y}{\partial \theta_i}\right)^2 \\ &= \sum_{i=1}^{n} \left[\left(\frac{\partial x}{\partial \theta_i}\right)^2 + \left(\frac{\partial y}{\partial \theta_i}\right)^2\right]. \end{aligned} \tag{4.7}$$

By considering the notations introduced in (4.4) and expanding the squares in (4.7), $\operatorname{tr}(\mathbf{J}\mathbf{J}^T)$ can be written as following:

$$\begin{aligned} \operatorname{tr}(\mathbf{J}\mathbf{J}^T) = \sum_{i=1}^{n} \Bigg[&\left(-\sum_{p=i}^{n} l_p \sin\left(\sum_{q=1}^{p} \theta_q\right)\right)^2 + \left(\sum_{p=i}^{n} l_p \cos\left(\sum_{q=1}^{p} \theta_q\right)\right)^2 \Bigg] \\ = \sum_{i=1}^{n}\sum_{p=i}^{n} &\left[l_p^2 \sin^2\left(\sum_{q=1}^{p} \theta_q\right) + l_p^2 \cos^2\left(\sum_{q=1}^{p} \theta_q\right)\right] + \\ 2\sum_{i=1}^{n-1} &\left[\sum_{p=i}^{n} l_p \sin\left(\sum_{q=1}^{p} \theta_q\right) \cdot \sum_{m=i+1}^{n} l_m \sin\left(\sum_{q=1}^{m} \theta_q\right) + \right. \\ &\left. \sum_{p=i}^{n} l_p \cos\left(\sum_{q=1}^{p} \theta_q\right) \cdot \sum_{m=i+1}^{n} l_m \cos\left(\sum_{q=1}^{m} \theta_q\right)\right]. \end{aligned} \tag{4.8}$$

For convenience, A and B are defined such that $\operatorname{tr}(\mathbf{J}\mathbf{J}^T) = A + B$. A is equal to the second row of (4.8) and B is equal to the third- and forth row of (4.8). A can be simplified by using the

trigonometric identity, $\sin^2(x) + \cos^2(x) = 1$:

$$\begin{aligned} A &= \sum_{i=1}^{n}\sum_{p=i}^{n}\left[l_p^2 \sin^2\left(\sum_{q=1}^{p}\theta_q\right) + l_p^2\cos^2\left(\sum_{q=1}^{p}\theta_q\right)\right] \\ &= \sum_{i=1}^{n}\sum_{p=i}^{n} l_p^2\left[\sin^2\left(\sum_{q=1}^{p}\theta_q\right) + \cos^2\left(\sum_{q=1}^{p}\theta_q\right)\right] \\ &= \sum_{i=1}^{n}\sum_{p=i}^{n} l_p^2 \\ &= \sum_{i=1}^{n} i l_i^2. \end{aligned} \tag{4.9}$$

Using the trigonometric identity, $\sin(x)\sin(y) + \cos(x)\cos(y) = \cos(x-y)$, B can be simplified:

$$\begin{aligned} B = 2\sum_{i=1}^{n-1}\Bigg[&\sum_{p=i}^{n} l_p \sin\left(\sum_{q=1}^{p}\theta_q\right)\cdot\sum_{m=i+1}^{n} l_m \sin\left(\sum_{q=1}^{m}\theta_q\right) + \\ &\sum_{p=i}^{n} l_p \cos\left(\sum_{q=1}^{p}\theta_q\right)\cdot\sum_{m=i+1}^{n} l_m \cos\left(\sum_{q=1}^{m}\theta_q\right)\Bigg] \\ = 2\sum_{i=1}^{n-1}\sum_{p=i}^{n}\sum_{m=i+1}^{n} &l_p l_m \cos\left(\sum_{q=1}^{p}\theta_q - \sum_{q=1}^{m}\theta_q\right). \end{aligned} \tag{4.10}$$

Noting that $m \geq p+1$, the last two summations in (4.10) can be written as one summation:

$$B = 2\sum_{i=1}^{n-1}\sum_{p=i}^{n}\sum_{m=i+1}^{n} l_p l_m \cos\left(-\sum_{q=p+1}^{m}\theta_q\right). \tag{4.11}$$

Finally, using the trigonometric identity $\cos(-x) = \cos(x)$, B can be expressed as:

$$B = 2\sum_{i=1}^{n-1}\sum_{p=i}^{n}\sum_{m=i+1}^{n} l_p l_m \cos\left(\sum_{q=p+1}^{m}\theta_q\right). \tag{4.12}$$

Since $\mathrm{tr}(\mathbf{J}\mathbf{J}^T) = A + B$, a final expression for $\mathrm{tr}(\mathbf{J}\mathbf{J}^T)$ is obtained with (4.9) and (4.12):

$$\mathrm{tr}(\mathbf{J}\mathbf{J}^T) = \sum_{i=1}^{n} i l_i^2 + 2\sum_{i=1}^{n-1}\sum_{p=i}^{n}\sum_{m=i+1}^{n} l_p l_m \cos\left(\sum_{q=p+1}^{m}\theta_q\right). \tag{4.13}$$

According to (4.13), The following relations between i, p, q hold:

$$\begin{cases} p \geq i \geq 1, \\ q \geq p+1. \end{cases} \tag{4.14}$$

Therefore, it can be concluded that $\mathrm{tr}(\mathbf{J}\mathbf{J}^T)$ is independent of θ_1 and the weighted Frobenius norm is given by:

$$\|\mathbf{J}\|_F = \sqrt{\frac{1}{2}\sum_{i=1}^{n} i l_i^2 + \sum_{i=1}^{n-1}\sum_{p=i}^{n}\sum_{m=i+1}^{n} l_p l_m \cos\left(\sum_{q=p+1}^{m}\theta_q\right)}. \tag{4.15}$$

□

4.1.2 The Weighted Frobenius Norm as a Measure of Manipulability

One of the reasons that manipulability indices are useful stems from the help they provide in avoiding singular configurations. From the analytic expression, (4.15), it can be concluded that this is not true for the weighted Frobenius norm. Consider, for example the point $\boldsymbol{\theta} = (0, \ldots, 0)$. This is an external singular configuration. When considering (4.15) it is clear that this is also a global maximum for $\|\mathbf{J}\|_F$. Therefore, it is not of interest to maximize $\|\mathbf{J}\|_F$. To minimize the weighted Frobenius norm is not of interest either since $\text{tr}(\mathbf{J}\mathbf{J}^T)$ is the sum of the eigenvalues. Because of this, it is of little or no use as a manipulability index and will not be used beyond this point. Similar arguments have previously been made in for example [5].

4.2 The Manipulability Measure

The manipulability measure was defined in Chapter 2 and is given by:

$$\mu = \sqrt{\det(\mathbf{J}\mathbf{J}^T)}. \tag{4.16}$$

4.2.1 First Angle Independence

Theorem 4.2. *The manipulability measure, μ, for a planar robotic arm is independent of the first angle, θ_1.*

Proof. The strategy of this proof is to show that the partial derivative of $\det(\mathbf{J}\mathbf{J}^T)$ with respect to θ_1 is zero, hence $\det(\mathbf{J}\mathbf{J}^T)$ is independent of θ_1. $\mathbf{J}\mathbf{J}^T$ is given by (4.6) and the determinant can thus be written as following:

$$\det(\mathbf{J}\mathbf{J}^T) = \sum_{i=1}^{n}\sum_{i=j}^{n}\left[\left(\frac{\partial x}{\partial \theta_i}\right)^2\left(\frac{\partial y}{\partial \theta_j}\right)^2 - \frac{\partial x}{\partial \theta_i}\frac{\partial y}{\partial \theta_i}\frac{\partial x}{\partial \theta_j}\frac{\partial y}{\partial \theta_j}\right]. \tag{4.17}$$

Considering the notations for the derivatives of the workspace coordinates, (4.4), note that the following hold for all i:

$$\begin{cases} \frac{\partial}{\partial \theta_1}\left(\frac{\partial x}{\partial \theta_i}\right) = -\frac{\partial y}{\partial \theta_i}, \\ \frac{\partial}{\partial \theta_1}\left(\frac{\partial y}{\partial \theta_i}\right) = \frac{\partial x}{\partial \theta_i}. \end{cases} \tag{4.18}$$

The derivative of $\det(\mathbf{J}\mathbf{J}^T)$ with respect to θ_1 is given by:

$$\begin{aligned} \frac{\partial}{\partial \theta_1}\left(\det(\mathbf{J}\mathbf{J}^T)\right) &= \frac{\partial}{\partial \theta_1}\sum_{i=1}^{n}\sum_{i=j}^{n}\left[\left(\frac{\partial x}{\partial \theta_i}\right)^2\left(\frac{\partial y}{\partial \theta_j}\right)^2 - \frac{\partial x}{\partial \theta_i}\frac{\partial y}{\partial \theta_i}\frac{\partial x}{\partial \theta_j}\frac{\partial y}{\partial \theta_j}\right] \\ &= \sum_{i=1}^{n}\sum_{i=j}^{n}\frac{\partial}{\partial \theta_1}\left[\left(\frac{\partial x}{\partial \theta_i}\right)^2\left(\frac{\partial y}{\partial \theta_j}\right)^2\right] - \sum_{i=1}^{n}\sum_{i=j}^{n}\frac{\partial}{\partial \theta_1}\left[\frac{\partial x}{\partial \theta_i}\frac{\partial y}{\partial \theta_i}\frac{\partial x}{\partial \theta_j}\frac{\partial y}{\partial \theta_j}\right]. \end{aligned} \tag{4.19}$$

For simplicity, A and B are defined such that $\frac{\partial}{\partial \theta_1}\left(\det(\mathbf{J}\mathbf{J}^T)\right) = A + B$ where A equals the first two sums and B the second two sums in (4.19). A can be simplified using the chain- and product

rule:

$$\begin{aligned} A &= \sum_{i=1}^{n}\sum_{i=j}^{n} \frac{\partial}{\partial\theta_1}\left[\left(\frac{\partial x}{\partial\theta_i}\right)^2\left(\frac{\partial y}{\partial\theta_j}\right)^2\right] \\ &= \sum_{i=1}^{n}\sum_{i=j}^{n} 2\left[\left(\frac{\partial x}{\partial\theta_i}\right)\left(\frac{\partial y}{\partial\theta_j}\right)^2 \cdot \frac{\partial}{\partial\theta_1}\left(\frac{\partial x}{\partial\theta_i}\right) + \left(\frac{\partial x}{\partial\theta_i}\right)^2\left(\frac{\partial y}{\partial\theta_j}\right)\cdot\frac{\partial}{\partial\theta_1}\left(\frac{\partial y}{\partial\theta_j}\right)\right] \\ &= \sum_{i=1}^{n}\sum_{i=j}^{n}\left[-2\frac{\partial x}{\partial\theta_i}\frac{\partial y}{\partial\theta_j}\frac{\partial y}{\partial\theta_j}\frac{\partial y}{\partial\theta_i} + 2\frac{\partial x}{\partial\theta_i}\frac{\partial x}{\partial\theta_i}\frac{\partial y}{\partial\theta_j}\frac{\partial x}{\partial\theta_j}\right]. \end{aligned} \tag{4.20}$$

B can also be simplified using the product rule:

$$\begin{aligned} B &= \sum_{i=1}^{n}\sum_{i=j}^{n}\frac{\partial}{\partial\theta_1}\left(\frac{\partial x}{\partial\theta_i}\frac{\partial y}{\partial\theta_i}\frac{\partial x}{\partial\theta_j}\frac{\partial y}{\partial\theta_j}\right) \\ &= \sum_{i=1}^{n}\sum_{i=j}^{n}\left(-\frac{\partial y}{\partial\theta_i}\frac{\partial y}{\partial\theta_i}\frac{\partial x}{\partial\theta_j}\frac{\partial y}{\partial\theta_j} + \frac{\partial x}{\partial\theta_i}\frac{\partial x}{\partial\theta_i}\frac{\partial x}{\partial\theta_j}\frac{\partial y}{\partial\theta_j} - \frac{\partial x}{\partial\theta_i}\frac{\partial y}{\partial\theta_i}\frac{\partial y}{\partial\theta_j}\frac{\partial y}{\partial\theta_j} + \frac{\partial x}{\partial\theta_i}\frac{\partial y}{\partial\theta_i}\frac{\partial x}{\partial\theta_j}\frac{\partial x}{\partial\theta_j}\right). \end{aligned} \tag{4.21}$$

Since $\frac{\partial}{\partial\theta_1}\left(\det(\mathbf{J}\mathbf{J}^T)\right) = A + B$, the expressions for A and B gives:

$$\begin{aligned} \frac{\partial}{\partial\theta_1}\left(\det(\mathbf{J}\mathbf{J}^T)\right) &= \sum_{i=1}^{n}\sum_{i=j}^{n}\left(-2\frac{\partial x}{\partial\theta_i}\frac{\partial y}{\partial\theta_i}\frac{\partial y}{\partial\theta_j}\frac{\partial y}{\partial\theta_j} + 2\frac{\partial x}{\partial\theta_i}\frac{\partial x}{\partial\theta_i}\frac{\partial x}{\partial\theta_j}\frac{\partial y}{\partial\theta_j} + \frac{\partial y}{\partial\theta_i}\frac{\partial y}{\partial\theta_i}\frac{\partial x}{\partial\theta_j}\frac{\partial y}{\partial\theta_j} - \right. \\ &\qquad \left. \frac{\partial x}{\partial\theta_i}\frac{\partial x}{\partial\theta_i}\frac{\partial x}{\partial\theta_j}\frac{\partial y}{\partial\theta_j} + \frac{\partial x}{\partial\theta_i}\frac{\partial y}{\partial\theta_i}\frac{\partial y}{\partial\theta_j}\frac{\partial y}{\partial\theta_j} - \frac{\partial x}{\partial\theta_i}\frac{\partial y}{\partial\theta_i}\frac{\partial x}{\partial\theta_j}\frac{\partial x}{\partial\theta_j}\right) \\ &= \sum_{i=1}^{n}\sum_{i=j}^{n}\left(-\frac{\partial x}{\partial\theta_i}\frac{\partial y}{\partial\theta_i}\frac{\partial y}{\partial\theta_j}\frac{\partial y}{\partial\theta_j} + \frac{\partial x}{\partial\theta_i}\frac{\partial x}{\partial\theta_i}\frac{\partial x}{\partial\theta_j}\frac{\partial y}{\partial\theta_j} + \frac{\partial y}{\partial\theta_i}\frac{\partial y}{\partial\theta_i}\frac{\partial x}{\partial\theta_j}\frac{\partial y}{\partial\theta_j} - \frac{\partial x}{\partial\theta_i}\frac{\partial y}{\partial\theta_i}\frac{\partial x}{\partial\theta_j}\frac{\partial y}{\partial\theta_j}\right). \end{aligned} \tag{4.22}$$

The terms in (4.22) may be written with different sums:

$$\begin{aligned} \frac{\partial}{\partial\theta_1}\left(\det(\mathbf{J}\mathbf{J}^T)\right) &= \sum_{i=1}^{n}\sum_{i=j}^{n}\left(\frac{\partial x}{\partial\theta_i}\frac{\partial x}{\partial\theta_i}\frac{\partial x}{\partial\theta_j}\frac{\partial y}{\partial\theta_j} + \frac{\partial y}{\partial\theta_i}\frac{\partial y}{\partial\theta_i}\frac{\partial x}{\partial\theta_j}\frac{\partial y}{\partial\theta_j}\right) - \\ &\qquad \sum_{i=1}^{n}\sum_{i=j}^{n}\left(\frac{\partial y}{\partial\theta_i}\frac{\partial x}{\partial\theta_i}\frac{\partial y}{\partial\theta_j}\frac{\partial y}{\partial\theta_j} + \frac{\partial x}{\partial\theta_i}\frac{\partial y}{\partial\theta_i}\frac{\partial x}{\partial\theta_j}\frac{\partial x}{\partial\theta_j}\right). \end{aligned} \tag{4.23}$$

Note that the indices of the sums may be switched. By switching the indices of the second sums in (4.23), the following is obtained:

$$\begin{aligned} \frac{\partial}{\partial\theta_1}\left(\det(\mathbf{J}\mathbf{J}^T)\right) &= \sum_{i=1}^{n}\sum_{i=j}^{n}\left(\frac{\partial x}{\partial\theta_i}\frac{\partial x}{\partial\theta_i}\frac{\partial x}{\partial\theta_j}\frac{\partial y}{\partial\theta_j} - \frac{\partial x}{\partial\theta_i}\frac{\partial x}{\partial\theta_i}\frac{\partial x}{\partial\theta_j}\frac{\partial y}{\partial\theta_j} + \frac{\partial y}{\partial\theta_i}\frac{\partial y}{\partial\theta_i}\frac{\partial x}{\partial\theta_j}\frac{\partial y}{\partial\theta_j} - \frac{\partial y}{\partial\theta_i}\frac{\partial y}{\partial\theta_i}\frac{\partial x}{\partial\theta_j}\frac{\partial y}{\partial\theta_j}\right) \\ &= \sum_{i=1}^{n}\sum_{i=j}^{n} 0. \end{aligned} \tag{4.24}$$

Since all terms in (4.24) are zero it can be concluded that:

$$\frac{\partial}{\partial\theta_1}\left(\det(\mathbf{J}\mathbf{J}^T)\right) = 0. \tag{4.25}$$

This shows that μ is independent of θ_1. □

4.2.2 Convexity

Proposition 4.3. *The manipulability measure, μ, of a planar robotic arm manipulator is not a convex function.*

Proof. The proof is done using the definition of convexity and by contradiction. It will be shown that convexity does not hold for the points $\boldsymbol{\theta}_a = (0,\ldots,0)$, $\boldsymbol{\theta}_b = (0,\frac{\pi}{2},0,\ldots,0)$ and $\boldsymbol{\theta}_c = (0,\pi,0,\ldots,0)$. For $\boldsymbol{\theta}_b$, the following holds when considering (4.4):

$$\begin{cases} \frac{\partial x}{\partial\theta_1}\Big|_{\theta=\theta_b} = -\sum_{p=2}^{n} l_p, \\ \frac{\partial x}{\partial\theta_i}\Big|_{\theta=\theta_b} = -\sum_{p=i}^{n} l_p, & i\neq 1, \\ \frac{\partial y}{\partial\theta_1}\Big|_{\theta=\theta_b} = l_1, \\ \frac{\partial y}{\partial\theta_i}\Big|_{\theta=\theta_b} = 0, & i\neq 1. \end{cases} \tag{4.26}$$

From expression above it follows that:

$$\begin{aligned} \det(\mathbf{J}\mathbf{J}^T)\,|_{\theta=\theta_b} &= \left[\sum_{i=1}^{n}\left(\frac{\partial x}{\partial\theta_i}\right)^2\sum_{j=1}^{n}\left(\frac{\partial y}{\partial\theta_j}\right)^2 - \sum_{i=1}^{n}\left(\frac{\partial x}{\partial\theta_i}\frac{\partial y}{\partial\theta_i}\right)\sum_{j=1}^{n}\left(\frac{\partial x}{\partial\theta_j}\frac{\partial y}{\partial\theta_j}\right)\right]\Bigg|_{\theta=\theta_b} \\ &= l_1^2\left[\left(\sum_{p=2}^{n} l_p\right)^2 + \sum_{i=2}^{n}\left(\sum_{p=i}^{n} l_p\right)^2 - \left(\sum_{p=2}^{n} l_p\right)^2\right] \\ &= l_1^2\left[\left(\sum_{p=2}^{n} l_p\right)^2 + \sum_{i=3}^{n}\left(\sum_{p=i}^{n} l_p\right)^2\right] > 0. \end{aligned} \tag{4.27}$$

Expressions for $\boldsymbol{\theta}_a$ and $\boldsymbol{\theta}_c$ are obtained analogously:

$$\begin{cases} \frac{\partial x}{\partial\theta_i}\Big|_{\theta=\theta_a} = 0, \\ \frac{\partial y}{\partial\theta_i}\Big|_{\theta=\theta_a} = \sum_{p=i}^{n} l_p. \end{cases} \tag{4.28}$$

$$\begin{cases} \frac{\partial x}{\partial\theta_i}\Big|_{\theta=\theta_c} = 0, \\ \frac{\partial y}{\partial\theta_i}\Big|_{\theta=\theta_c} = -\sum_{p=i}^{n} l_p, & p\neq 1, \\ \frac{\partial y}{\partial\theta_1}\Big|_{\theta=\theta_c} = l_1 - \sum_{p=2}^{n} l_p. \end{cases} \tag{4.29}$$

Which for $\boldsymbol{\theta}_a$ leads to:

$$\det(\mathbf{J}\mathbf{J}^T)\mid_{\theta=\theta_a} = \sum_{i=1}^{n}\sum_{j=1}^{n}\left[0^2\left(\sum_{p=j}^{n} l_p\right)^2 - 0^2\left(\sum_{p=i}^{n} l_p\right)\left(\sum_{p=j}^{n} l_p\right)\right] = 0. \tag{4.30}$$

Similarly, the same result is obtained for $\boldsymbol{\theta}_c$:

$$\begin{aligned}\det(\mathbf{J}\mathbf{J}^T)\mid_{\theta=\theta_c} = 0^2\left[\left(l_1 - \sum_{p=2}^{n} l_p\right)^2 + \sum_{i=2}^{n}\left(\sum_{p=i}^{n} l_p\right)^2\right] - \\ 0^2\left[\left(l_1 - \sum_{p=2}^{n} l_p\right) - \sum_{i=2}^{n}\left(\sum_{p=i}^{n} l_p\right)\right]\left[\left(l_1 - \sum_{p=2}^{n} l_p\right) - \sum_{j=2}^{n}\left(\sum_{p=j}^{n} l_p\right)\right] = 0.\end{aligned} \tag{4.31}$$

Recall that a function, f, is convex if for any x, y in the set S, $f(\alpha x+(1-\alpha)y) \leq \alpha f(x)+(1-\alpha)f(y)$ holds $\forall\alpha \in [0,1]$. Now let $x = \boldsymbol{\theta}_a$, $y = \boldsymbol{\theta}_c$ and $\alpha = \frac{1}{2}$. Then the following is a necessary condition for μ to be convex:

$$\mu\left(\frac{1}{2}\boldsymbol{\theta}_a + \frac{1}{2}\boldsymbol{\theta}_c\right) \leq \frac{1}{2}\mu(\boldsymbol{\theta}_a) + \frac{1}{2}\mu(\boldsymbol{\theta}_c). \tag{4.32}$$

Recall that $\mu = \sqrt{\det(\mathbf{J}\mathbf{J}^T)}$ which together with (4.31) and (4.30) gives that $\mu(\boldsymbol{\theta}_a) = \mu(\boldsymbol{\theta}_c) = 0$. This together with the fact that $\frac{1}{2}\boldsymbol{\theta}_a + \frac{1}{2}\boldsymbol{\theta}_c = \boldsymbol{\theta}_b$ leads to an equivalent statement to (4.32):

$$\mu(\boldsymbol{\theta}_b) \leq 0. \tag{4.33}$$

But when considering (4.27) it is easily concluded that (4.33) is false which contradicts that μ is convex and therefore the proof is complete. □

4.3 The Condition Number

In chapter 2 the condition number, κ, was defined as:

$$\kappa = \sqrt{\frac{\lambda_{min}}{\lambda_{max}}}. \tag{4.34}$$

4.3.1 First Angle Independence

Theorem 4.4. *The condition number, κ, for a planar robotic arm is independent of the first angle, θ_1.*

Proof. According to the definition above, it is sufficient to prove that the eigenvalues, λ_{min} and λ_{max}, of $\mathbf{J}\mathbf{J}^T$ are independent of θ_1. Let a, b, c and d denote the elements in $\mathbf{J}\mathbf{J}^T$ such that:

$$\mathbf{J}\mathbf{J}^T = \begin{pmatrix} a & b \\ c & d \end{pmatrix}. \tag{4.35}$$

Then, the characteristic equation of $\mathbf{J}\mathbf{J}^T$ is:

$$\det\begin{pmatrix} a-\lambda & b \\ c & d-\lambda \end{pmatrix} = (a-\lambda)(d-\lambda) - bc = \lambda^2 - (a+d)\lambda + (ad-bc) = 0. \tag{4.36}$$

The solution to (4.36) is given by:

$$\lambda = \frac{a+d}{2} \pm \sqrt{\frac{(a+d)^2}{4} - ad + bc}. \tag{4.37}$$

Using that $\text{tr}(\mathbf{J}\mathbf{J}^T) = a + d$ and that $\det(\mathbf{J}\mathbf{J}^T) = ad - bc$, (4.37) can be simplified to:

$$\lambda = \frac{\text{tr}(\mathbf{J}\mathbf{J}^T)}{2} \pm \sqrt{\frac{\left(\text{tr}(\mathbf{J}\mathbf{J}^T)\right)^2}{4} - \det(\mathbf{J}\mathbf{J}^T)}. \tag{4.38}$$

According to Theorem 4.1 and Theorem 4.2, the determinant and trace of $\mathbf{J}\mathbf{J}^T$ is independent of θ_1. Considering this together with (4.38), it is clear that both eigenvalues are independent of θ_1. Hence, κ is independent of θ_1. □

4.3.2 The Condition Number as a Measure of Manipulability

The gains of using the condition number as a measure of manipulability is due to the help it provides in avoiding singular configurations. At singular configurations the condition number converges to zero. However, it does not give any information about the magnitude of the manipulability. Thus, if optimization is performed from the viewpoint of optimizing κ this can lead to reduced manipulability of the configuration. This is illustrated in the schematic Figure 4.1. Therefore, the condition number will not be used as an objective function in the numerical optimization but it will be used as a supplement to the manipulability measure.

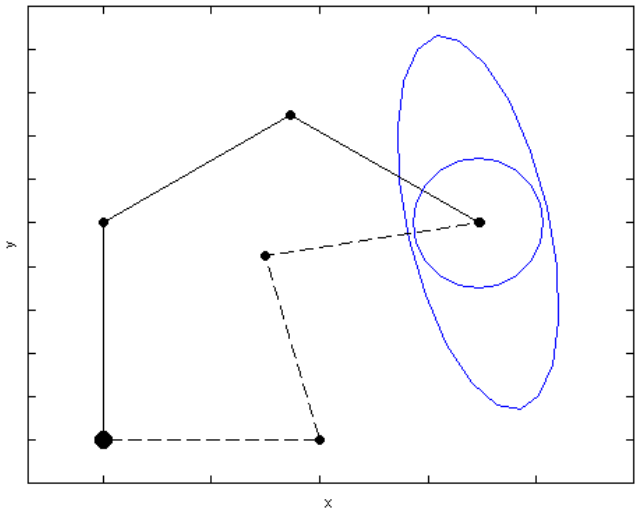

Figure 4.1: Schematic figure illustrating the disadvantage of the condition number. The figure contains two different arm configurations together with their respective ellipses. The smaller circle within the ellipse will give a higher value of κ while the ellipse has better manipulability in all directions.

Chapter 5

Optimization of a Three Link Planar Arm

In this chapter the manipulability measure, μ, will be optimized for a three link planar arm under certain constraints. Three links are chosen since the results are easily visualized. Observe that the problems are analogous for higher number of links.

5.1 Specifications and the Objective Function

Consider a three link planar robotic arm manipulator model. The link lengths are for simplicity set to:

$$l_1 = l_2 = l_3 = 1. \tag{5.1}$$

Recall that the manipulability measure is independent of θ_1. Therefore, the function to maximize is $\mu(\theta_2, \theta_3)$ but $\boldsymbol{\theta} = (\theta_1, \theta_2, \theta_3)^T$ is still considered as the variable in order for the connection between the feasible set and the joint space to be clear. Analytically, an implicit expression for μ is obtained from (2.11) and (2.19) as following:

$$\begin{aligned}\mu^2 &= \frac{1}{2}l_1^2 \cdot l_2^2 + (l_1^2 + l_2^2) \cdot l_3^2 + l_1 \cdot l_2 \cdot l_3^2 \cdot \cos(\theta_2) - \frac{1}{2}l_1^2 \cdot l_2^2 \cdot \cos(2\theta_2) + l_1 \cdot l_2^2 \cdot l_3 \cdot \cos(\theta_3) - \\ &\quad l_2^2 \cdot l_3^2 \cos(2\theta_3) - l_1^2 \cdot l_3^2 \cos(2\theta_2 + 2\theta_3) - l_1^2 \cdot l_2 \cdot l_3 \cos(2\theta_2 + \theta_3) - l_1 \cdot l_2 \cdot l_3^2 \cos(\theta_2 + 2\theta_3) \\ &= \frac{3}{2} + \cos(\theta_2) - \frac{1}{2}\cos(2\theta_2) + \cos(\theta_3) - \frac{1}{2}\cos(2\theta_3) - \\ &\quad \cos(2\theta_2 + 2\theta_3) - \cos(2\theta_2 + \theta_3) - \cos(\theta_2 + 2\theta_3).\end{aligned} \tag{5.2}$$

Note that since $\cos(-x) = \cos(x)$, there is an important symmetry. If $(\hat{\theta}_2, \hat{\theta}_3)$ is an optimal solution, then $-(\hat{\theta}_2, \hat{\theta}_3)$ is also an optimal solution. Some constant terms and the square of μ may be disregarded and a simpler function, $\tilde{\mu}$, to optimize is obtained:

$$\begin{aligned}\tilde{\mu} &= \cos(\theta_2) - \frac{1}{2}\cos(2\theta_2) + \cos(\theta_3) - \frac{1}{2}\cos(2\theta_3) - \\ &\quad \cos(2\theta_2 + 2\theta_3) - \cos(2\theta_2 + \theta_3) - \cos(\theta_2 + 2\theta_3).\end{aligned} \tag{5.3}$$

The problems in this chapter are solved using the built in function *fmincon* in MATLAB with $\tilde{\mu}$ as objective function. μ is used for plots and tables. For more background theory regarding numerical optimization, see [12].

5.2 Unconstrained Optimization

The mathematical formulation of the unconstrained optimization problem can be written as following:

$$\begin{bmatrix} \text{minimize} & -\tilde{\mu}(\boldsymbol{\theta}) \\ \text{s.t.} & \boldsymbol{\theta} \text{ free} \end{bmatrix}. \tag{5.4}$$

In this problem, there are no constraints on the joint variables. Observe that $\boldsymbol{\theta}$ free is equivalent to the constraints $\theta_i \in [0, 2\pi]$, $i = 1, 2, 3$. This is due to the periodicity of μ and $\tilde{\mu}$. According to Theorem 3.1, since the set $\theta_i \in [0, 2\pi]$, $i = 1, 2, 3$ is compact, there exists a minimum to this unconstrained optimization problem. The joint- and workspace for the equivalent problem are illustrated in Figure 5.1. The joint space can be considered as the feasible region for this optimization problem.

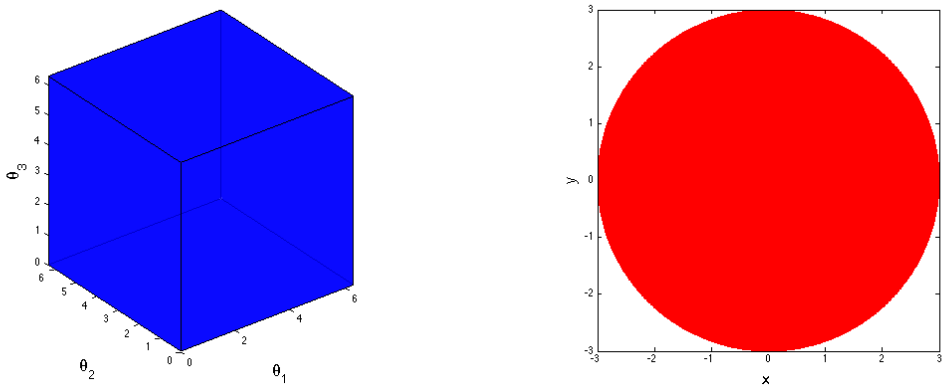

(a) The joint space

(b) The workspace

Figure 5.1: Joint- and workspace for the unconstrained optimization problem. The joint space consists of all possible angle configurations and the workspace is the set of all possible end-effector positions.

The numerically obtained solution to problem (5.4) corresponds to a radius from the origin of the manipulator because of the first angle independence in μ and $\tilde{\mu}$. The radius is calculated using direct kinematics. The results of the optimization is found in Table 5.1 and a plot of the manipulability measure is found in Figure 5.2. The numerically obtained solutions has been validated using Newtons method with a grid of start guesses to find all the stationary points.

Table 5.1: The numerically obtained angles and radius corresponding to the maximum value of the manipulability measure.

radius, R	θ_2(rad)	θ_3(rad)	μ
2.15	$\pm$ 0.78	$\pm$ 1.13	2.63

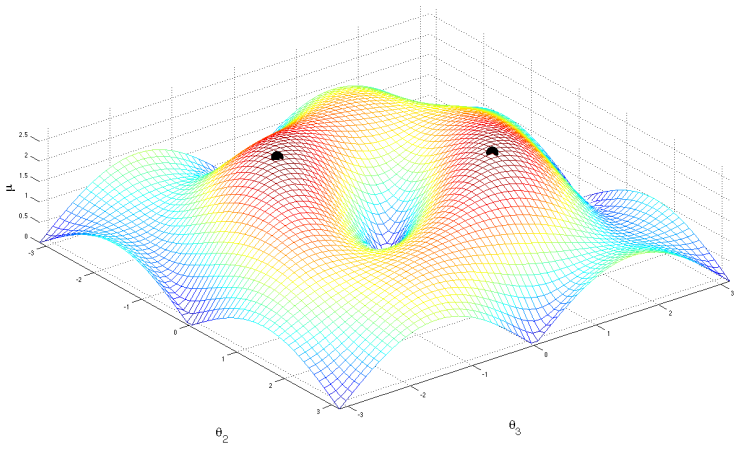

Figure 5.2: A plot of the manipulability measure, μ. The two numerically obtained optimal points for problem (5.4) are marked.

5.3 Radius Constraints

Another problem is to constrain the robotic arm end-effector to be positioned at a certain radius from the origin i.e., the norm of the forward kinematic function is constrained. This can be formulated as an optimization problem:

$$\begin{bmatrix} \text{minimize} & -\tilde{\mu}(\boldsymbol{\theta}) \\ \text{s.t.} & ||\mathbf{f}|| = R \end{bmatrix}. \tag{5.5}$$

By solving (5.5) for different radii in the workspace, the numerically obtained solution as a function of the radius is acquired. The result is plotted in Figure 5.3. The radius with highest obtained value is consistent with the radius obtained in the unconstrained optimization, see Table 5.1.

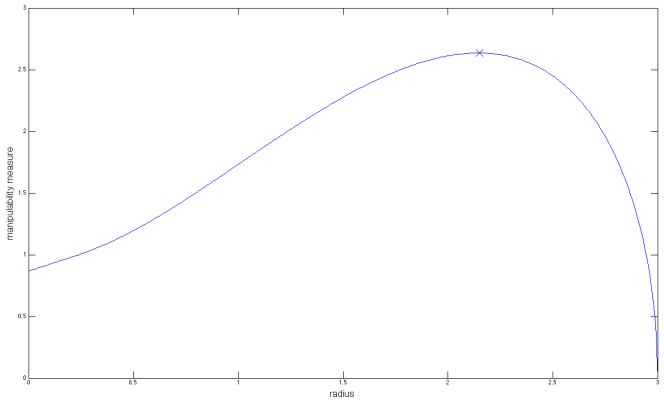

Figure 5.3: The numerically obtained optimal solution for different radii. The radius that gives the highest value of manipulability measure is marked.

Feasible sets for $\boldsymbol{\theta}$ exists for each non-singular radius. The feasible set may be regarded as a line in the (θ_2, θ_3)-space or, since μ is independent of θ_1, as a surface in the joint space. As an example, the feasible region for the optimal radius, $R = 2.15$ is illustrated in Figure 5.4.

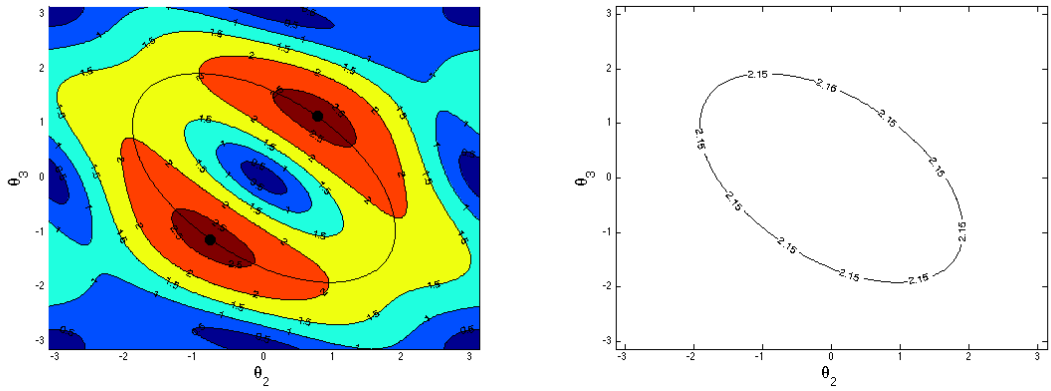

(a) A contour plot **(b)** The feasible region

Figure 5.4: The feasible set of θ_2, θ_3 when $R = 2.15$. (a) shows the contour plot of the manipulability measure with the feasible set and optimal points and (b) illustrates the feasible set without the contour.

Examples of manipulability ellipsoids for several, numerically obtained, optimal configurations are found in Figure 5.5. To show the relation between the ellipsoids, ellipsoids for $\boldsymbol{\theta}$ and $-\boldsymbol{\theta}$ are plotted. The $(-\boldsymbol{\theta})$-configuration corresponds to a mirror image of the $\boldsymbol{\theta}$-configuration. The corresponding configurations share the same value of the manipulability measure but have high manipulability in different directions.

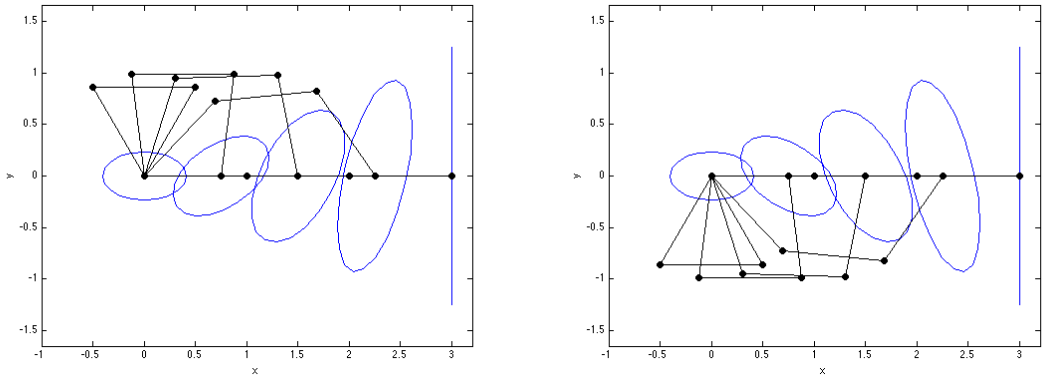

(a) Ellipsoids for the first solution **(b)** Ellipsoids for the mirror image of the first solution

Figure 5.5: Velocity manipulability ellipsoids for the numerically obtained optimal solutions for $R = 0, 0.75, ..., 3.0$. The ellipsoids are scaled with a factor 3 for aesthetic reasons.

5.4 Angular Constraints

By only allowing $\theta_i \in [-\frac{\pi}{2}, \frac{\pi}{2}], i = 1, 2, 3$, the optimization problem can be written as:

$$\begin{bmatrix} \text{minimize} & -\tilde{\mu}(\boldsymbol{\theta}) \\ \text{s.t.} & \theta_i \leq \frac{\pi}{2} \\ & -\theta_i \leq \frac{\pi}{2} \\ & i = 1, 2, 3 \end{bmatrix}. \tag{5.6}$$

The constraints on $\boldsymbol{\theta}$ in (5.6) gives the joint- and workspace illustrated in Figure 5.6. Note that the constraints are linear and give a compact set of feasible $\boldsymbol{\theta}$. Therefore, a minimum once again exists according to Theorem 3.1.

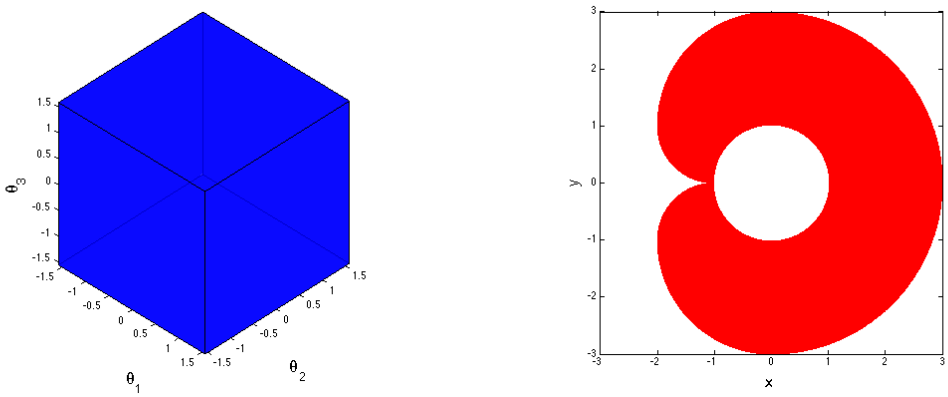

(a) The joint space **(b)** The workspace

Figure 5.6: Joint- and workspace with anglular constraints.

Since the feasible set still contains the obtained solution in the unconstrained optimization problem, this numerical optimization gives the same result. The result is found in Table 5.1. The manipulability measure for the feasible region is illustrated in Figure 5.7.

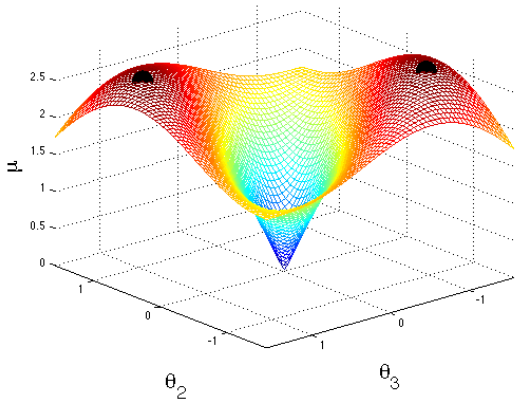

Figure 5.7: The manipulability for the feasible set of (θ_2, θ_3). Numerically obtained optimal solutions are marked.

5.5 Angular and Radius Constraints

The optimization problem considered in this section can be written as:

$$\begin{bmatrix} \text{minimize} & -\tilde{\mu}(\boldsymbol{\theta}) \\ \text{s.t.} & \theta_i \leq \frac{\pi}{2} \\ & -\theta_i \leq \frac{\pi}{2} \\ & ||\mathbf{f}|| = R \\ & i = 1, 2, 3 \end{bmatrix}. \tag{5.7}$$

(5.7) is solved for different radii. The results are found in Table 5.2. It also lists the value of the corresponding condition number, κ. Because of the angular constraints, $R \in [1, 3]$. Figure 5.8 illustrates the feasible sets for two different radii.

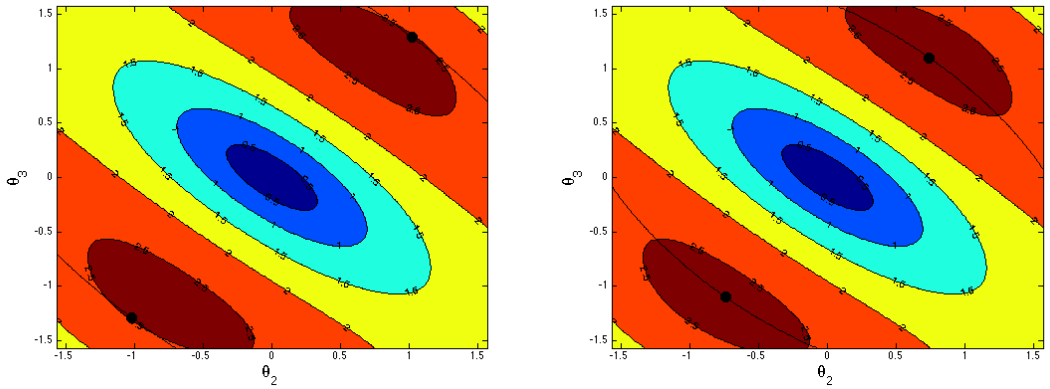

(a) $R = 1.8$ **(b)** $R = 2.2$

Figure 5.8: Contour plots of the manipulability measure with feasible sets for (θ_2, θ_3) marked in black. The numerically obtained optimal points are also marked.

Table 5.2: Some values of the optimal μ with corresponding κ and angle configurations for different radii. Observe that, κ is decreasing with the radius.

radius, R	θ_2(rad)	θ_3(rad)	μ	κ
1.0	1.57	1.57	1.73	0.58
1.4	1.30	1.44	2.18	0.54
1.8	1.02	1.29	2.52	0.44
2.2	0.74	1.10	2.63	0.33
2.6	0.47	0.80	2.30	0.22
3.0	0.00	0.00	0.00	0.00

Corresponding velocity and force ellipsoids for the configurations in Table 5.2 are plotted in Figure 5.9.

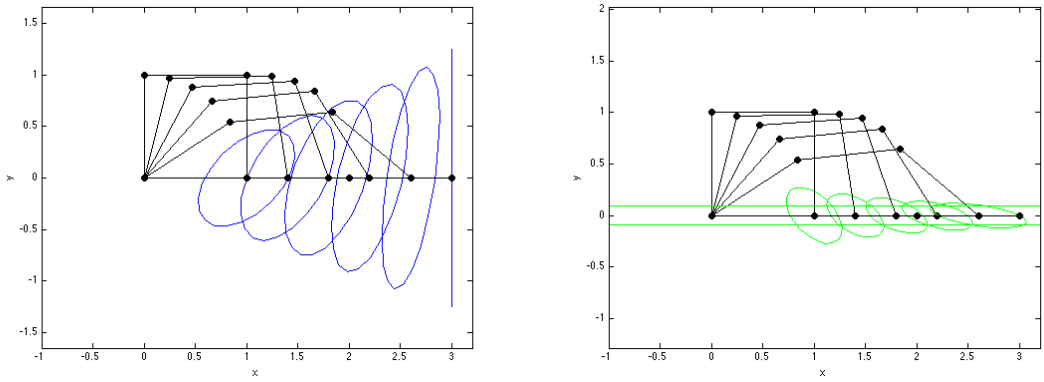

(a) Velocity ellipsoids

(b) Force ellipsoids

Figure 5.9: Velocity- and force ellipsoids for different $\boldsymbol{\theta}$-configurations with angle constraints. Once again, the axes are scaled with a factor 3 for aesthetic reasons. The horizontal axis for the force ellipsoids corresponding to $||\mathbf{f}|| = 3$ does not fit in the plot since it goes to infinity.

Chapter 6

Trajectory Optimization in Joint Space

In this chapter, a method of obtaining a path with good manipulability through the joint space is described. The method is presented for several examples.

6.1 The Trajectory Optimization Method

6.1.1 The Path-Polynomial

There are different ways to approach the problem of optimizing a path for a robotic arm manipulator. Firstly, one may optimize the path in either the joint space or in the workspace. The two options each have separate advantages and disadvantages. This has been discussed in previous work on the subject, see [13]. To summarize, the joint space is preferable if there are no obstacles in the workspace since the joints are controlled by the manipulator. It also allows for faster computations since no inverse kinematics is used. However, obstacles in the workspace are difficult to express in the joint space which makes path planning in the workspace preferable in that case. Since an obstacle free workspace is considered, this is outside the scope of this report. See [13] and [14] for further details regarding trajectory optimization in the workspace.

In this model, the path through the joint space is studied since no obstacles are considered. The path will be given by the *path-polynomial*, $\mathbf{\Theta}(t)$:

$$\mathbf{\Theta}(t) = (\Theta_1(t), ..., \Theta_n(t))^T, \tag{6.1}$$

where:

$$\Theta_i = \sum_{j=0}^{k} a_{ij} t^j. \tag{6.2}$$

The path-polynomial is a n dimensional vector consisting of polynomials of degree k where n is the dimension of the joint space i.e., the number of joints in the robot arm manipulator. The variable $t : 0 \to 1$, is the parameter actuating the path and a_{ij} are the coefficients for the polynomials. Constructing paths of polynomials are appropriate since polynomials are C^∞ i.e., all derivatives are continuous. This gives continuous angular velocities and angular accelerations along the path.

In order to obtain a path, a start- and end configuration must be defined. The start configuration is defined as: $\boldsymbol{\theta}_s = (\theta_{1s}, ..., \theta_{ns})^T$ and the end configuration as $\boldsymbol{\theta}_f = (\theta_{1f}, ..., \theta_{nf})^T$. This may be written as constraints on the path-polynomial:

$$\begin{cases} \boldsymbol{\Theta}(0) = \boldsymbol{\theta}_s, \\ \boldsymbol{\Theta}(1) = \boldsymbol{\theta}_f. \end{cases} \tag{6.3}$$

The constraints may be rewritten as constraints on the coefficients a_{ij}:

$$\begin{cases} a_{i0} = \theta_{is}, \\ \sum_{j=0}^{k} a_{ij} = \theta_{if}, \\ i = 1, ..., n. \end{cases} \tag{6.4}$$

Observe that these are linear constraints on a_{ij}.

6.1.2 The Objective Function

When defining the objective function, the following two factors are considered:

i The length of the path throughout the joint space i.e., how much the angles are changed throughout the path.

ii The value of the manipulability measure for all points in the path.

The validity of these factors has previously been discussed in [13] but in that case a path was constructed in the workspace. The factors considered for the joint space optimization problem are however analogous and still valid.

The first factor is taken into account by using the formula for arc length, $\Delta\boldsymbol{\Theta}$, in a n-dimensional joint space:

$$\Delta\boldsymbol{\Theta}(t) = \sqrt{\sum_{q=1}^{n} \left(\frac{\partial \Theta_q}{\partial t} \right)^2}. \tag{6.5}$$

To account for the value of the manipulability measure, μ, in all points, the multiplicative inverse is used in order to formulate a minimization problem. Since $t : 0 \to 1$, the objective function, g is defined as:

$$g = \int_{t=0}^{1} \frac{\Delta\boldsymbol{\Theta}(t)}{\mu(\boldsymbol{\Theta}(t))} dt = \int_{t=0}^{1} \frac{1}{\mu(\boldsymbol{\Theta}(t))} \sqrt{\sum_{q=1}^{n} \left(\frac{\partial \Theta_q}{\partial t} \right)^2} dt. \tag{6.6}$$

To optimize (6.6) is to minimize the arc length while taking a path with high manipulability. Note that the value of g grows very large if the path goes close to singularities. Therefore, the function is well defined in the sense that it avoids singularities.

6.1.3 Problem Formulation

The optimization problem consists of obtaining an optimal path-polynomial in terms of minimizing (6.6). The path-polynomial must satisfy the conditions (6.4). Therefore, the optimization

problem for a planar robotic arm with n joints and a path-polynomial of degree k is given by:

$$\left[\begin{array}{ll} \text{minimize} & g(a_{ij}) \\ \text{s.t.} & \boldsymbol{\Theta}(t) \in \mathcal{J}, \forall t \in [0,1] \\ & \sum_{j=0}^{k} a_{ij} = \theta_{if} \\ & a_{i0} = \theta_{is} \\ & i = 1, ..., n \end{array}\right]. \tag{6.7}$$

Where g is given by (6.6) and $\boldsymbol{\Theta}$ is given by (6.1) and (6.2). $\mathcal{J}$ denotes the specified joint space.

In the examples presented in this chapter, the robotic arm manipulator will once again be modeled as a three link planar arm. The link lengths are given by:

$$l_1 = l_2 = l_3 = 1. \tag{6.8}$$

A feasible path, $\boldsymbol{\Theta}_0(t)$, is obtained by calculating a straight line from the start- to the end configuration. This is used as a start guess for the numerical optimization.

$$\boldsymbol{\Theta}_0(t) = \begin{pmatrix} \theta_{1s} \\ \theta_{2s} \\ \theta_{3s} \end{pmatrix} + \begin{pmatrix} \theta_{1f} - \theta_{1s} \\ \theta_{2f} - \theta_{2s} \\ \theta_{3f} - \theta_{3s} \end{pmatrix} \cdot t. \tag{6.9}$$

6.2 A Comparison Between Different Degrees of Polynomials

To show that this method is valid, it is of importance that the paths given by different degrees of polynomials converge. Polynomials of degree 1 to 6 will be considered and compared for two arbitrary examples. The first path will be given by:

$$\begin{array}{l} \boldsymbol{\theta}_s \to \boldsymbol{\theta}_f, \\ \boldsymbol{\theta}_s = (0, -3.0, -2.0)^T, \\ \boldsymbol{\theta}_f = (\pi, 0.1, 1.4)^T. \end{array} \tag{6.10}$$

For this problem, (6.7) gives us the following optimization problem:

$$\left[\begin{array}{ll} \text{minimize} & g(a_{ij}) \\ \text{s.t.} & \sum_{j=0}^{k} a_{ij} = \theta_{if} \\ & a_{i0} = \theta_{is} \\ & i = 1, 2, 3 \end{array}\right]. \tag{6.11}$$

Here, the optimization is performed for $k = 2, ..., 6$. The results for different k are found in Table 6.1. g denotes the numerically obtained optimal value of the objective function and Δg denotes the difference between the value of g and g for the previous degree. Notice that the value of g is decreasing with increasing degree and also that $|\Delta g|$ is decreasing, indicating convergence.

Table 6.1: Comparison between the optimal solution for different degrees of path-polynomial.

degree	g	$\lvert\Delta g\rvert$
1	2.7218	
2	2.4600	0.2618
3	2.3168	0.1432
4	2.2542	0.0626
5	2.2376	0.0166
6	2.2361	0.0015

In Figure 6.1, the paths are illustrated both in the (θ_2, θ_3)-space and the workspace. In the (θ_2, θ_3)-space, a contour plot of the manipulability measure is also plotted. The numerical solutions for polynomials of degrees 3 or more yields approximately the same path, also indicating convergence. This can be seen in Figure 6.1.

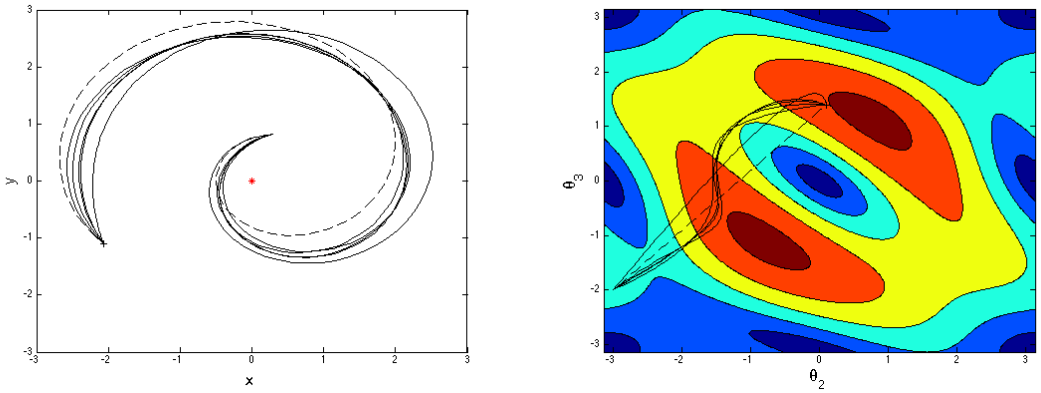

(a) Path in workspace

(b) Path in the (θ_2, θ_3)-space

Figure 6.1: Numerically obtained paths in the work- and (θ_2, θ_3)-space for different polynomial. The dashed line represent the linear solution.

For the second example, the following path will be considered:

$$\begin{aligned} &\boldsymbol{\theta}_s \rightarrow \boldsymbol{\theta}_f, \\ &\boldsymbol{\theta}_s = (0, -1.1, -1.6)^T, \\ &\boldsymbol{\theta}_f = (\tfrac{\pi}{2}, 0.5, 1.5)^T. \end{aligned} \tag{6.12}$$

This problem is the same as (6.11) with different start- and end configurations. The result of this numerical optimization is found Table 6.2 and the paths are illustrated in Figure 6.2.

Table 6.2: Comparison between the numerical solution for different degrees of path-polynomial.

degree	g	$\lvert\Delta g\rvert$
1	3.9420	
2	1.1371	2.8049
3	1.1185	0.0186
4	1.1143	0.0042
5	1.1114	0.0030
6	1.1114	0.0000

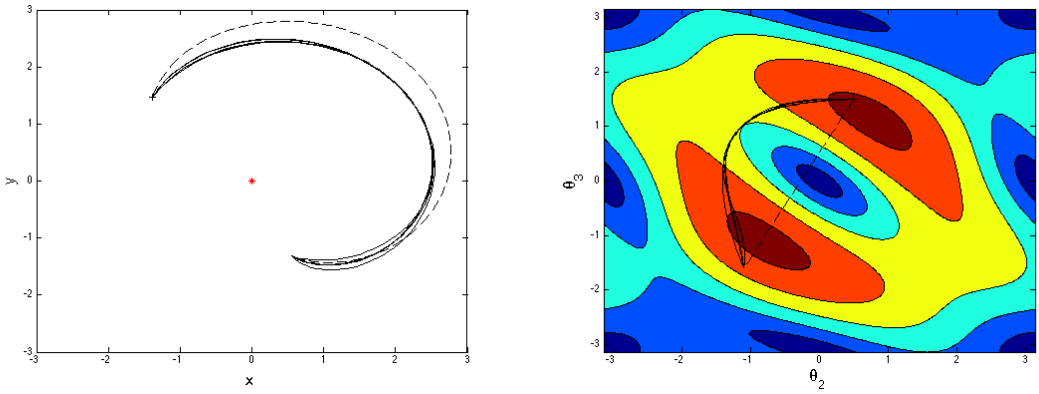

(a) Path in workspace

(b) Path in the (θ_2, θ_3)-space

Figure 6.2: Numerically obtained paths in the work- and (θ_2, θ_3)-space for different polynomial. The dashed line represent the linear solution.

6.3 A Comparison Between the Linear and the Numerically Obtained Solution

To illustrate the improvements that the numerically optimized path yields, a comparison between the linear and the optimized paths are conducted. The start- and end configurations for this last example are chosen as:

$$\begin{aligned} &\boldsymbol{\theta_s} \rightarrow \boldsymbol{\theta_f}, \\ &\boldsymbol{\theta_s} = (0, 1.5, -2)^T, \\ &\boldsymbol{\theta_f} = (\pi, -2, 2)^T. \end{aligned} \tag{6.13}$$

The degree of the polynomial is chosen as 6 since it is previously shown that a degree of 6 is sufficient. No angular constraints are used.

The optimization problem can thus be formulated as:

$$\begin{bmatrix} \text{minimize} & g(a_{ij}) \\ \text{s.t.} & \sum_{j=0}^{6} a_{ij} = \theta_{if} \\ & a_{i0} = \theta_{is} \\ & i = 1, 2, 3 \end{bmatrix}. \tag{6.14}$$

The results are found below. Table 6.3 displays the values for the path-polynomial coefficients. Note that the constraints in (6.14) are satisfied.

Table 6.3: Coefficients for the numerically obtained path-polynomial.

	j	0	1	2	3	4	5	6
a_{1j}		0	1.05	2.30	0.92	-0.26	-0.60	-0.27
a_{2j}		1.50	-4.19	0.84	-0.54	-0.86	-0.09	1.34
a_{3j}		-2.00	0.61	1.05	0.89	0.55	0.44	0.44

The path in the workspace and in the (θ_2, θ_3)-space are illustrated in Figure 6.3.

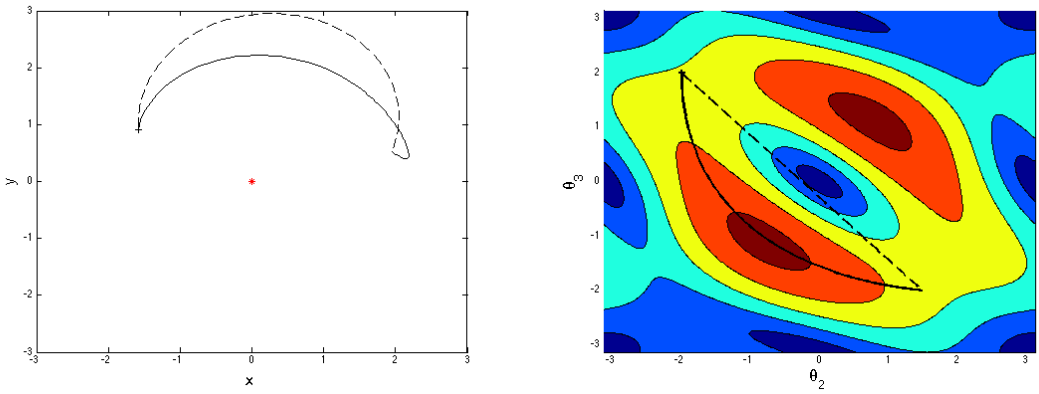

(a) Path in workspace

(b) Path in the (θ_2, θ_3)-space

Figure 6.3: The linear- and numerically obtained path in the work- and (θ_2, θ_3)-space. The dashed line represent the linear joint space solution while the non-dashed line represent the numerical solution.

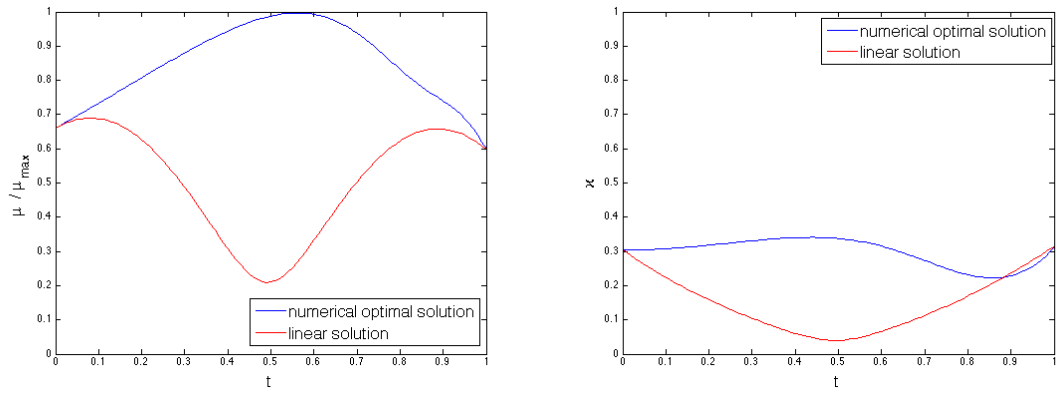

(a) Manipulability measure as a function of t

(b) Condition number as a function of t

Figure 6.4: Manipulability measure and condition number throughout the path.

Figure 6.4 displays the manipulability measure and condition number throughout the path. The improvements in manipulability are clear. Observe that the configuration is considerably closer to a singular configuration for the linear solution.

Table 6.4 tabulates different comparisons between the obtained optimal- and the linear solution. The linear solution is denoted by a subscript L. The first column is the ratio between the value of the objective function for the linear and numerically obtained solution. The second column is the ratio between the path lengths in the joints space. The third and forth column describes the quotas between the value of μ and κ integrated over the path for the two solutions.

Table 6.4: Comparison between the optimal- and linear solution.

$\frac{g_L}{g}$	$\frac{\Delta\boldsymbol{\theta}_L}{\Delta\boldsymbol{\theta}}$	$\frac{\int_{t=0}^{1}\mu_L(t)dt}{\int_{t=0}^{1}\mu(t)dt}$	$\frac{\int_{t=0}^{1}\kappa_L(t)dt}{\int_{t=0}^{1}\kappa(t)dt}$
0.27	0.92	0.60	0.50

Chapter 7

Discussion and Conclusions

This report has studied the optimization of planar robotic arms, which have been modeled and analyzed. Formulating the optimization problems and imposing various types of constraints have lead to problems concerning the task of maximizing the manipulability.

The modeling of the robotic arm is relatively crude in the sense that it is only based on kineostatics which makes it hard to implement with dynamical properties. However, the studied methods still hold vital information which can be implemented in the design of robotic manipulators. The studied optimization problems show the versatility of problems which can be formulated. It also demonstrates the gains which can be made from manipulability optimization. The constraints considered in Chapter 5 occurs naturally in industrial applications. The angular constraints corresponds to a robotic arm which can not make full turns around its joints. The solution to the radius constraint problems yields information regarding the optimal distance for the robotic manipulator to work in.

The analytical result regarding the first angle independence of the manipulability indices confirms the validity of the chosen indices. First angle independence is a natural property and if the studied manipulability indices did not share this feature they could have been discarded. This report has discussed several manipulability indices but the numerical optimization has been performed using the *manipulability measure*, μ, as objective function since this index describes the manipulability of the structure in the best way. The *weighted Frobenius norm*, $\|\mathbf{J}\|_F$, is not sufficient because it does not avoid singular configurations. The *condition number*, κ, is not a proficient measure of manipulability since it only provides the ratio between the manipulability in different directions and does not consider the magnitude of the manipulability. The condition number however holds information regarding proximity to singular configurations which is of interest.

Depending on the robotic task at hand several types of improvement can be found for the design and usage of planar robotic arms. Notably problems concerning finding the optimal path for a manipulator have been formulated and solved by optimizing a polynomial describing the path in the joint space. Describing the optimal path in the joint space have several perks regarding the simplicity of the modeling but a major drawback is the difficulty of describing and thus avoiding obstacles. The method of finding the optimal path polynomial described in joint space is thus restricted to the case of an obstacle free workspace. It can be concluded that the method of optimizing a path-polynomial is valid since the paths converge with increasing degrees of the polynomials. Since the generated path in the joint space consists of polynomials, the joint velocities and accelerations will be smooth.

Appendix A

Rewriting an Arbitrary Ellipsoid on Standard Form

According to [15], an ellipsoid in $\mathbb{R}^n$ centered in the origin can be written on standard form as:

$$\left(\frac{x_1}{a_1}\right)^2 + \left(\frac{x_2}{a_2}\right)^2 + \cdots + \left(\frac{x_n}{a_n}\right)^2 = 1. \tag{A.1}$$

The direction of the principal axes are given by x_1, x_2, ..., x_n with lengths a_1,..., a_n respectively. An arbitrary ellipsoid may also be expressed using matrix notion:

$$\mathbf{x}^T\mathbf{A}\mathbf{x} = 1, \tag{A.2}$$

where $\mathbf{A}$ is a $n \times n$ positive semidefinite matrix and $\mathbf{x} = (x_1, \ldots, x_n)^T$. The matrix $\mathbf{A}$ may be rewritten using diagonalization:

$$\mathbf{A} = \mathbf{P}\mathbf{D}\mathbf{P}^{-\mathbf{1}}, \tag{A.3}$$

where $\mathbf{D}$ is a diagonal matrix with diagonal entries $\lambda_1 \ldots$, λ_n, which are the eigenvalues of $\mathbf{A}$. $\mathbf{P}$ is a matrix consisting of unit eigenvectors, $\mathbf{u}_1, \ldots, \mathbf{u}_n$, of the matrix $\mathbf{A}$ as columns. Note that since $\mathbf{P}$ is an orthogonal matrix it holds that: $\mathbf{P}^{-1} = \mathbf{P}^T$. Inserting expression (A.3) in (A.2) yields:

$$\mathbf{x}^T(\mathbf{P}\mathbf{D}\mathbf{P}^{-\mathbf{1}})\mathbf{x} = 1. \tag{A.4}$$

By defining $\mathbf{x}' = \mathbf{P}^{-\mathbf{1}}\mathbf{x}$, which gives that $\mathbf{x}'^T = (\mathbf{P}^{-1}\mathbf{x})^T = \mathbf{x}^T\mathbf{P}$, expression (A.4) can be rewritten:

$$\mathbf{x}'^T\mathbf{D}\mathbf{x}' = 1 \iff \lambda_1 x_1'^2 + \cdots + \lambda_n x_n'^2 = 1. \tag{A.5}$$

Equation (A.5) is the equation for an ellipsoid on standard form and a comparison with equation (A.1) gives us the principal axes of the ellipsoid as x_1',..., x_n' with lengths $\frac{1}{\sqrt{\lambda_1}}$,..., $\frac{1}{\sqrt{\lambda_n}}$ respectively. The principal axes are thus governed by the eigenvectors and the square root of the reciprocal eigenvalues of $\mathbf{A}$. Recall that an arbitrary positive semidefinite square matrix $\mathbf{A}$ share the same eigenvectors but have reciprocal eigenvalues with its inverse. The ellipse (A.2) is thus governed by the eigenvalues and eigenvectors of $\mathbf{A}^{-1}$.

Appendix B

Calculating the Volume of an n-Dimensional Ellipsoid Using the Determinant

The volume, V, of a n-dimensional ellipsoid can be written as:

$$V = K \prod_{i=1}^{n} a_i. \tag{B.1}$$

Where K is a real positive constant depending on the dimension of the ellipsoid and $a_1, \ldots, a_n$ are the lengths of the principal axes. From Appendix A, it is known that the equation for an ellipsoid can be rewritten using diagonalization:

$$\mathbf{x}^T\mathbf{A}\mathbf{x} = \mathbf{x}^T(\mathbf{P}\mathbf{D}\mathbf{P}^{-1})\mathbf{x} = \mathbf{x'}^T\mathbf{D}\mathbf{x'} = 1, \tag{B.2}$$

and that the lengths of the principal axes are given by $a_i = \frac{1}{\sqrt{\lambda_i}}$. Using this, (B.1) may be rewritten using the determinant in the following way:

$$\prod_{i=1}^{n} \frac{1}{\lambda_i} = \frac{1}{\det(\mathbf{D})} = \frac{1}{\det(\mathbf{P^{-1}AP})} = \frac{1}{\det(\mathbf{P^{-1}})}\frac{1}{\det(\mathbf{A})}\frac{1}{\det(\mathbf{P})} = \frac{1}{\det(\mathbf{A})} = \det(\mathbf{A^{-1}}) \Rightarrow$$

$$\Rightarrow \prod_{i=1}^{n} a_i = \prod_{i=1}^{n} \frac{1}{\sqrt{\lambda_i}} = \sqrt{\det(\mathbf{A^{-1}})} \Rightarrow V = K\sqrt{\det(\mathbf{A^{-1}})}. \tag{B.3}$$

Bibliography

[1] B. Kamrani, V. Berbyuk, D. Wäppling, X. Feng and H. Andersson. *Optimal Usage of Robot Manipulators.* Robot Manipulators Trends and Development, INTECH, 2010.

[2] B. Siciliano, L. Sciavicco, L. Villani and G. Oriolo. *Robotics: Modelling, Planning and Control.* Springer, second edition, 2011.

[3] R. M. Murray, Z. Li and S. S. Sastry. *A Mathematical Introduction to Robotic Manipulation.* CRC Press, 1994.

[4] B. Siciliano and O. Khatib. *Springer Handbook of Robotics.* Springer, first edition, 2008.

[5] J. Kim and P. K. Khosla. *Dexterity Measures for Design and Control of Manipulators.* International Workshop on Intelligent Robots and Systems IROS '91, 1991.

[6] D. Emiris and V. Tourassis. Journal of Intelligent & Robotic Systems, Volume 8, Issue 2, 1993.

[7] T. Yoshikawa. *Dynamic Manipulability of Robot Manipulators.* International Journal of Robotics Research, Volume 4, Issue 2, 1985.

[8] J. T. Wen and L. S. Wilfinger. *Kinematic Manipulability of General Constrained Rigid Multibody Systems.* Transactions on Robotics and Automation, Volume 15, Issue 3, 1999.

[9] P. Chiacchio, Y. Bouffard-Vercelli and F. Pierrot. *Force Polytope and Force Ellipsoid for Redundant Manipulators.* Journal of Robotic Systems, Volume 14, Issue 8, 1997.

[10] I. Griva, S. G. Nash and A Sofer. *Linear and Nonlinear Optimization.* Society for Industrial and Applied Mathematics, second edition, 2009.

[11] W. Rudin. *Principles of Mathematical Analysis.* McGraw-Hill, third edition, 1976.

[12] J. Nocedal and S. Wright. *Numerical Optimization.* Springer, 2000.

[13] X. F. Zha and X. Chen. *Path Coordination Planning and Control in Robotic Material Handling and Processing.* In Industrial Robotics: Programming, Simulation and Applications, pages 231-254, 2007.

[14] B. Ryuh. *Robot Trajectory Planning Using the Curvature Theory of Ruled Surfaces.* Ph.D Thesis, Purdue University, 1989.

[15] H. Anton. *Elementary Linear Algebra.* Wiley, 2005.